Journal of proteome research

pubs.acs.org/jpr

Article

Skeletal Muscle Proteome Modifications following Antibiotic-Induced Microbial Disturbances in Cancer Cachexia

Mathilde Simonson, Gwendal Cueff, Morgane M. Thibaut, Christophe Giraudet, Jérôme Salles, Christophe Chambon, Yves Boirie, Laure B. Bindels, Marine Gueugneau, and Christelle Guillet*

Cite This: *J. Proteome Res.* 2024, 23, 2452−2473

Read Online

ACCESS | Metrics & More | Article Recommendations | Supporting Information

ABSTRACT: Cancer cachexia is an involuntary loss of body weight, mostly of skeletal muscle. Previous research favors the existence of a microbiota-muscle crosstalk, so the aim of the study was to evaluate the impact of microbiota alterations induced by antibiotics on skeletal muscle proteins expression. Skeletal muscle proteome changes were investigated in control (CT) or C26 cachectic mice (C26) with or without antibiotic treatment (CT-ATB or C26-ATB, n = 8 per group). Muscle protein extracts were divided into a sarcoplasmic and myofibrillar fraction and then underwent label-free liquid chromatography separation, mass spectrometry analysis, Mascot protein identification, and METASCAPE platform data analysis. In C26 mice, the atrogen *mafbx* expression was 353% higher than CT mice and 42.3% higher than C26-ATB mice. No effect on the muscle protein synthesis was observed. Proteomic analyses revealed a strong effect of antibiotics on skeletal muscle proteome outside of cachexia, with adaptative processes involved in protein folding, growth, energy metabolism, and muscle contraction. In C26-ATB mice, proteome adaptations observed in CT-ATB mice were blunted. Differentially expressed proteins were involved in other processes like glucose metabolism, oxidative stress response, and proteolysis. This study confirms the existence of a microbiota-muscle axis, with a muscle response after antibiotics that varies depending on whether cachexia is present.

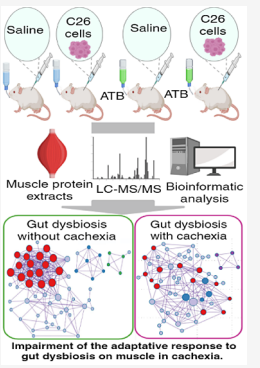

KEYWORDS: *skeletal muscle, proteomics, antibiotics, cancer cachexia, microbial disturbances*

INTRODUCTION

Cancer cachexia is a multifactorial disorder characterized by the involuntary loss of body weight that results predominantly from loss of skeletal muscle and fat mass.[1] In this situation, skeletal muscle atrophy is recognized as an independent risk factor for the impairment of quality of life[2] and poor survival in cancer patients,[3] because it contributes to reduced chemotherapy treatment tolerance[4] and increased surgical complications.[5]

The loss of skeletal muscle mass results, in part, from an imbalance between muscle protein breakdown and synthesis.[6] Indeed, increased inflammation related to the disease together with circulating tumoral factors contribute to the activation of signaling pathways controlling skeletal muscle proteolysis systems, in particular the autophagy lysosome[7] and ubiquitin proteasome system.[8] One of the main signaling pathways involved in the dysregulation of protein metabolism in cancer cachexia is the Akt-FoxO signaling axis, which directly regulates the expression of the main upregulated genes in catabolic conditions, the atrophy-related genes, *muscle ring finger 1* (*murf1*) and *muscle atrophy f-box* gene (*mafbx*).[9] Anabolic signaling pathways implicating Insulin Growth Factor 1[10] (IGF1) and mammalian Target of Rapamycin (mTOR)[11] are also impaired, leading to a decrease in the skeletal muscle protein synthesis rate.[12] In addition to the global investigation of skeletal muscle protein metabolism regulation, some studies based on the exploration of skeletal muscle protein expressions through a proteomic approach have highlighted metabolic pathways that could be affected during cancer cachexia.[13] For instance, proteomic analyses in the quadriceps of mice with severe cachexia revealed that two-thirds of the proteins identified were downregulated and involved in muscle energy metabolism, more specifically mitochondrial function (the tricarboxylic acid or TCA cycle, mitochondrial respiratory chain, glycolysis, and fatty acid beta oxidation).[14] In a rodent model of cancer cachexia, the Colon-26 Carcinoma Tumor-bearing mouse (the C26 mouse),[15] proteomic analyses of skeletal muscle showed an upregulation of acute phase reaction proteins and complement responses, and a downregulation of proteins involved in mitochondria oxidative phosphorylation as well as ribosomal proteins.[16] Finally, skeletal muscle proteomic analyses in C26 mice with moderate (10% weight loss) and severe (20% weight loss) cachexia revealed altered pathways such as extracellular matrix regulation and fibrin formation, Mitogen activated protein kinase (MAPK) signaling, inflammatory response (via Toll Like Receptor or TLR regulation and

Received: February 27, 2024
Revised: June 2, 2024
Accepted: June 2, 2024
Published: June 19, 2024

https://doi.org/10.1021/acs.jproteome.4c00143
J. Proteome Res. 2024, 23, 2452−2473

complement signaling), and ribosome and translation pathways.[13] Several pathways were identified in severe cachexia, including mitochondrial metabolic alterations (TCA cycle, mitochondrial electron transport, and pyruvate metabolism). Overall, these proteomic studies in rodent models of cancer cachexia show major disrupted pathways regulating skeletal muscle energy metabolism, muscle structure, and immune and inflammation responses.

Among the mechanisms involved in the regulation of skeletal muscle protein metabolism, such as a disruption in the balance of protein synthesis and breakdown or changes in protein expression, emerging evidence in the literature suggests that gut microbiota play a role in the setup of skeletal muscle alterations during cancer cachexia. Indeed, gut microbiota dysbiosis in the BaF3 mice model of leukemia is correlated with cachectic characteristics such as skeletal muscle mass loss and upregulation of atrophy markers genes.[17] In this mouse model, administration of *L. reuteri* improved the loss of muscle mass and reduced mRNA expression of muscle atrophy markers.[17] In the C26 mouse model, impairments in gut microbiota composition lead to increased gut barrier permeability.[18] Metabolically, microbial dysbiosis in cachectic mice might be linked with decreased intestinal *de novo* protein synthesis[12] and amino acid uptake,[19] which might contribute to alter muscle protein metabolism downstream.[11] Even if key findings strongly suggest a gut-muscle axis in cancer cachexia, current research has not fully uncovered the mechanisms leading to the involvement of microbial dysbiosis in skeletal muscle atrophy and the dysregulation of muscle protein metabolism and expression during cachexia.

The aim of this study is, therefore, to explore the effect of microbiota modulation using broad-spectrum antibiotic treatment on skeletal muscle protein metabolism and protein expression in the C26 mouse cancer cachexia model.

EXPERIMENTAL SECTION

Cell Culture

Before *in vivo* implantation, colon carcinoma 26 (C26) cells were maintained in high-glucose Dulbecco's modified Eagle's medium supplemented with 10% fetal bovine serum (Capricorn, South America), 100 μg/mL streptomycin, and 100 IU/mL penicillin (Gibco, Belgium) at 37 °C with 5% CO_2.

Mouse Experiments

Ethical Aspects. The experiments were approved by the local Ethical Committee of the Université Catholique de Louvain and performed in accordance with ethical guidelines. Housing conditions were as specified by the Belgian Law of 29 May 3, 2013, regarding the protection of laboratory animals (Agreement No. LA1230314).

Experimental Procedure. Male CD2F1 mice (7 weeks old, Charles River Laboratories, Italy) were housed in a specific pathogen-free environment in individually ventilated cages (2 mice/cage) with a 12 h light/dark cycle and fed *ad libitum* with an irradiated chow diet (AO4−10, 2.9 kcal/g, SAFE, France). After a one-week acclimatization, mice were allocated into two groups (n = 16/group): one group with antibiotics (vancomycin 0.29 mM; neomycin 0.95 mM, Meropenem 0.206 mM) added to the drinking water (ATB) and one group without antibiotics. After 7 days of antibiotic treatment, half of the mice in each group received a subcutaneous injection (intrascapular) of saline (sham) or C26 cells (1×10^6 cells in 0.1 mL saline). All C26-implanted mice displayed a visible tumor mass after 7 days. In total, 4 groups of mice were studied: CT control mice, CT-ATB control mice treated with antibiotics treatment, C26 mice implanted with C26 cells, and C26-ATB mice implanted with implant C26 cells and treated with antibiotics (n = 8 per group). Nine days after cancer cell implantation and 16 days after the beginning of antibiotic treatment, mice were fasted for 5 h prior to necropsy. 50 min before necropsy, mice were injected intraperitoneally with a flooding dose of L-[^{13}C]-Valine (Eurisotop, Saint-Aubin, France) at 300 μmol/100 g of body weight (n = 7 per group).

Sampling. Feces were collected before the initiation of the antibiotic treatment, the day of the saline or C26 cell injection, and the day of necropsy and stored at −80 °C. Blood samples were collected from the vena cava and portal vein following anesthesia (isoflurane gas, Abbot, Belgium), centrifuged, and snap frozen in liquid nitrogen. Gastrocnemius and tibialis muscles were collected, weighed, snap frozen in liquid nitrogen, and then stored at −80 °C until further analyses.

Fecal Microbiome Analyses. DNA was extracted from stools following the protocol Q,[20] which uses the QIAamp DNA Stool Mini Kit (Qiagen, Germany) and includes a bead-beating step. Treatment with RNase A was performed (10 mg/mL, Thermo Fisher Scientific, USA). DNA concentration was determined, and purity (A260/A280) was checked using a NanoDrop 2000 instrument (Thermo Fisher Scientific, USA). Absolute quantification of the total bacterial load was performed by qPCR using the primers Bacteria Universal P338F (ACTCCTACGGGAGGCAGCAG) and P518r (ATTACCGCGGCTGCTGG)[21] as described in Supporting Information 1. Universal bacterial DNA was then quantified as previously described using *L. acidophilus* (DSM 20079 04−14) as the standard bacteria.[22] Samples were diluted to 0.10 g/μL or used pure when nanodrop concentration was less than 10 ng/μL. All samples (0.1 ng/μL) were run in duplicate in a single 96-well reaction plate. Final concentrations were as follows: cDNA 2 μL/25 μL, primers 300 nM, and SyberGreen mix 1X (MeteorTaq DNA polymerase, dNTP, RT buffer, MgCl2 4 mM, SYBR Green I, ROX passive reference, and stabilizers, as provided by the manufacturer). Thermocycling conditions were as follows: initiation step at 95 °C for 2 min; cycling stage at 95 °C for 30 s, 60 °C for 30 s, 72 °C for 30 s, 40 cycles; melt curve stage at 95 °C for 1 s, 65 °C for 20 s, increment of 0.1 °C every 1 s until reaching 95 °C. Threshold was manually adjusted to reach the linear range of the log-fluorescent curves, and CT values were determined using the QuantStudio Software (Version 1.4.3, Applied Biosystems, The Netherlands). Absolute quantification was achieved through the inclusion of a standard curve (performed in duplicate) on each plate generated by diluting DNA from pure culture of *L. acidophilus* NCFM (5-fold serial dilution). Cell counts were determined by plating and expressed as the "colony-forming unit" (CFU) before DNA isolation. Taxonomic composition was assessed using 16S rRNA gene sequencing of the cecal content DNA V4 and V5 regions as previously described.[23] Sequencing procedures, as well as bioinformatics and biostatistics analyses, are detailed in Supporting Information 1. Raw sequences can be found in the SRA database (project ID: PRJNA881269).

Immunohistochemistry Analyses. Gastrocnemius muscle was mounted with tissue freezing medium (OCT) before being snap frozen using isopentane and then stored at −80 °C. Cross sections (10 μm thick) were performed using a cryostat at −20 °C, and were labeled as previously described.[24] Briefly, sections were labeled with antilaminin-α1 (L9393,

https://doi.org/10.1021/acs.jproteome.4c00143
J. Proteome Res. 2024, 23, 2452−2473

Table 1. Primer List

gene name	forward	reverse
igfbp5[a]	AGAGCTACGGCGAGCAAA	TCTGCGGTCCTTCTTCACA
igf1	GCTCTTCAGTTCGTGTGTGG	CACAATGCCTGTCTGAGGTG
irs1	CTCAACAGCAGTCCCTACCAC	GAGGATTTGCTGAGGTCATTT
klf15	CAAGAACCCAGCAGCAGAAC	AACTCATCTGAGCGGGAAAA
mafbx	ATGCACACTGGTGCAGAGAG	TGTAAGCACACAGGCAGGTC
murf1	ACGAGAAGAAGAGCGAGC	CTTGGCACTTGAGAGGAA
redd1	GTCTGCAGCCAGAGAAGAGG	CCCATCCAGGTATGAGGAG

[a]*Igfbp5*: Insulin Growth Factor Binding Protein 5. *Irs1*: Insulin Receptor Substrate 1. *Klf15*: Krüppel-like factor 15. *redd1*: Regulated in Development and DNA Damage 1.

Sigma-Aldrich) to outline the fibers and resolved with corresponding secondary antibodies conjugated to Alexa-Fluor 488 (Invitrogen, Cergy-Pontoise, France). Imaging was performed at 10× (Zeiss, Okerkochen, Germany) and processed using ImageJ (1.53c, java version 1.8 0_265) to obtain the fibers' cross-sectional area. Five fields, each containing more than 100 fibers, were analyzed per muscle.

Fractional Synthesis Muscle Protein Rate (FSR). Gastrocnemius muscle free amino acids and total proteins were extracted as previously described.[25] Briefly, muscle proteins were hydrolyzed using 6M-HCl, and the constituent amino acids were purified by cation exchange chromatography (Dowex 50W 8X; Bio-Rad Laboratories, Hercules, CA, USA). Amino acids were eluted in 4M-NH4OH, dried in a SpeedVac (Savant Instruments, Inc. Holbrook, NY, USA), and derivatized as their N-acetyl-propylderivative. L-[^{13}C]-Valine enrichment (Ei) was measured using a gas-chromatography-combustion-isotope ratio mass spectrometer system (GC-C-IRMS, μGas System; Fisons Instruments,VG Isotech, Middlewich, UK). One animal from each group was not injected with stable isotope tracers to determine the natural Ei in L-[^{13}C]-Valine. The following formula was used to calculate the fractional synthesis rate:

$$\text{FSR } (\%.h^{-1}) = ((\text{Ei of [13C] derived from Valine in total muscle proteins} - \text{natural Ei of [13C] derived from Valine}) \times 100)/(\text{Ei of [13C] derived from Valine in free amino acid pool} \times \text{incorporation time in hour})$$

Gastrocnemius mRNA Analyses. RNA isolation, cDNA generation, and real-time qPCR were executed as described previously.[19] The ribosomal protein L6 (Rpl6) gene was chosen as the reference gene for all tissues. The primer sequences for the targeted mouse genes are detailed in Table 1.

Gastrocnemius Proteomic Analyses. *Proteomic Sample Preparation.* Skeletal muscles (CT, C26, CT-ATB and C26-ATB, n = 8 per group) were prepared for proteomic analyses as previously described.[26] Briefly, 50 mg of gastrocnemius was homogenized on ice using an Ultra-Turrax homogenizer (IKA Labortechnik, Staufen, Germany) and extraction buffer (40 mM Tris-HCL, Sigma #T3253; 2 mM EDTA 0.5 M, Sigma #03659; protease inhibitor solution, Sigma #P8340). Muscle homogenate was divided into two fractions: the sarcoplasmic protein-enriched extract and the myofibrillar protein-enriched extract. Samples were centrifuged at 10000g at 4 °C, and the supernatant or sarcoplasmic protein-enrichment extract was obtained. The myofibrillar protein-enriched extract was obtained after the pellet was resolubilized (50 mM Tris-HCL; 8 mM urea), then incubated for 2 h on ice and centrifuged for 5 min at 5000g at 4 °C. Both fractions were conserved at −80 °C. Protein samples were then migrated on a 1D-SDS PAGE gel to obtain a protein band as described previously.[27] After excision and processing of each band, the proteins were digested with trypsin at a ratio of 1:75 and the peptides obtained were dried then resolubilized in 20 μL of a 0.1% TFA solution containing standard QC peptides (1 pmol, Isotopologues, PROMEGA).

Label-Free LC−MS/MS Analyses. The myofibrillar and sarcoplasmic fractions of each mouse were subjected once to the mass spectrometry analysis, with eight biological replicates per group and a randomized sample order. 6 μL of hydrolysate was separated by an acetonitrile gradient (ACN/FA 99.9/0.1) ranging from 4 to 25% for 50 min in a Nano HPLC. Then the samples were electrosprayed in a Q-ORBITRAP HFX mass spectrometer (ThermoScientific).

Protein Identification and Quantification. The separated peptides were analyzed in the MS/MS DDA mode, top N20 for identification, and quantification by Progenesis LCProQI (Nonlinear, Waters) using Mascot (V251) and Peaks (X) identification software. The search and identification parameters in the mouse database (55408 seq, unip 202102) were 10 ppm and 0.05 Da for parent and fragment ions, respectively. A protein was validated when at least 2 unique peptides from the protein had a significant score with a false positive rate (FPR) below 1%. Protein quantification by LCProQI was based on the average abundance of the 4 most intense peptides of each protein (3 or 2 for proteins identified with only 2 or 3 peptides). This step resulted in the elimination of outliers (1 mouse) and samples with insufficient alignment scores between soluble and myofibrillar extracts of the same mouse. CT: sham-implanted mice (n = 8), CT-ATB: sham-implanted mice treated by antibiotics (n = 6), C26: C26-implanted mice (n = 8), C26-ATB: C26-implanted mice treated with antibiotics (n = 7). The mass-spectrometry proteomics data have been deposited to the ProteomeXchange Consortium via the PRIDE partner repository[28] with the data set identifier PXD043918. Potential contaminants such as casein, keratin, or trypsin were excluded. Then statistical analysis was performed using the "combined analyzed mode" option, which combines the myofibrillar and sarcoplasmic protein quantifications, enabling statistics to be calculated for the whole proteomic experiment. One-way ANOVA were performed on the abundances of each protein quantified in this way, between the CT and C26, CT and CT-ATB, or C26 and C26-ATB groups. A protein was considered differentially accumulated if its q-value was below 0.05 (name given to the adjusted p-values found using an optimized false discovery rate approach with a rate <0.05).

Proteomic Analysis Workflow. Principal component analysis (PCA) was conducted on the identified, differentially accumulated proteins using Factominer on R (R software, version 4.2.3). Using the *Mus musculus* database, the selected proteins were biologically analyzed using METASCAPE online tools (Current version v3.5.20230501) for enrichment pathway

https://doi.org/10.1021/acs.jproteome.4c00143
J. Proteome Res. 2024, 23, 2452−2473

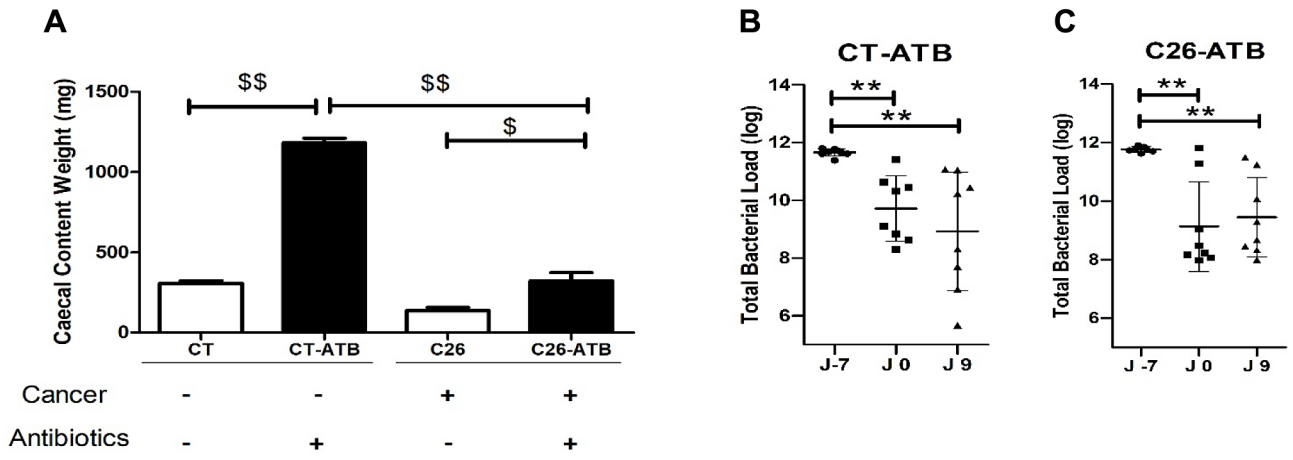

Figure 1. Impact of antibiotic treatment on cecal content weight and total bacterial load. (A) Cecal content on the day of necropsy. (B,C) Total bacteria count evolution expressed as the logarithmic charge, before antibiotic treatment (Day −7), at the time of C26 injection (Day 0), and on the day of necropsy (Day 9) for CT-ATB (B) and C26-ATB mice (C). $N = 8$ per group. CT: sham-implanted mice, CT-ATB: sham-implanted mice treated by antibiotics, C26: C26-implanted mice, C26-ATB: C26-implanted mice treated with antibiotics. Statistically significant differences between groups are shown with $ when Kruskal–Wallis and Dunn's post-test was used or * when a two-way ANOVA followed by Bonferroni post-test was used. One symbol: $p < 0.05$; 2 symbols: $p < 0.01$.

and protein network analyses. METASCAPE[29] recognizes genes without the necessity of user specification using their gene name and annotates their Gene Ontology[30] (GO) biological processes (BP) by curating them automatically from databases like UniProt.[29] Enrichment analyses in METASCAPE narrow down the redundant GO BP processes using Kappa similarities and classify the processes according to their p-value.[29] We used a custom background consisting of our identified proteins, a minimum overlap of 3, a p-value cut off of 0.05, and a minimum enrichment of 1.5 for the pathway and process enrichment.

Then, protein network analyses were performed using the Molecular Complex Detection (MCODE) algorithm,[31] which extracts the most densely connected proteins in the protein interaction network graph and generates a cluster for these proteins. This approach is combined in METASCAPE with the biological processes curated, in order to derive a putative role for the cluster.[29] We used a minimum network size of 3 for the protein–protein interaction study.

Finally, Cytoscape (Java 11.06, version 3.9.1) with the WikiPathway application (3.3.10) was used to illustrate which pathways contained differentially expressed proteins in the C26 and C26-ATB mice.

Statistical Analyses Outside of Proteomics. Results are expressed as mean ± sem. Statistical analyses were performed using GraphPad Prism 5.0, except for microbiome data analyses. $p < 0.05$ was considered to be significant. Outliers were removed using the Grubbs test. Normality was assessed using D'Agostino and Pearson omnibus normality test.

Analyses over time among CT, CT-ATB, and C26 and C16-ATB groups were performed using repeated measures mixed-model ANOVA, with Bonferroni-post-tests.

Analyses at a given time point were analyzed with a two-way ANOVA followed by Bonferroni post-tests when results followed a normal distribution; when it was not the case, a Kruskal–Wallis test was used with a Dunn's post-test. Except otherwise indicated, stars were used when a two-way ANOVA followed by Bonferroni post-tests was performed and dollar symbol was when the Kruskal–Wallis test was used with a Dunn's post-test, with 1 symbol for a p value below 0.05; 2 for a p value below 0.01, and 3 for a p value below 0.001.

RESULTS AND DISCUSSION

Antibiotics Treatment and C26 Implantation Affect the Gut Microbiota Composition

Cecal content was significantly increased in mice treated with antibiotics and significantly decreased in animals with cachexia, with a significant difference between C26 and C26-ATB mice (Figure 1A). The total bacterial load over time was reduced as early as 7 days after beginning the antibiotic treatment (day 0) both for the CT-ATB and C26-ATB groups, but with heterogeneous responses within the groups (Figure 1B,C). These data together with the lack of difference in water intake between groups during the experiment (Figure S1) are strong elements indicating that antibiotics were adequately consumed throughout the experiment.

Looking at these results, the increase in cecal content is a classical feature of microbial disturbances outside of cachexia, in mice treated with broad-spectrum antibiotic cocktails as early as 10 days after beginning treatment.[32,33] During cachexia, there is a significant decrease in cecal content in C26 mice compared to the control mice,[19] regardless of anorexia,[34] which is the dominant effect here in the cachectic mice. Other studies using broad-spectrum antibiotics, including vancomycin and neomycin, up to three or 4 weeks have shown insufficient lowering of the total bacterial load, with only certain families of bacteria being depleted[32] and others persisting such as *Enterobacteriaceae*.[35]

To explore the heterogeneous results in total bacteria content, gut microbiota composition was assessed on the days of injection and necropsy using 16S rRNA gene sequencing. Alpha diversity evenness indexes were significantly decreased in groups treated by antibiotics compared to the untreated mice (Figure S2). PCA at the family level showed that the major variance in the samples was due to the antibiotic treatment (Figure S3). Analyses focusing on CT and C26 mice revealed an increased relative abundance of *Enterobacteriaceae* in the C26 group, which is a classical feature of this model[34] (Figure S3 and Table S1). Overall, mice without antibiotic treatment presented the *Firmicutes* and *Bacteroides* phyla and the *Lachnospiraceae, Lactobacillaceae*, and *Ruminococcaceae* families at day 0 and day

https://doi.org/10.1021/acs.jproteome.4c00143
J. Proteome Res. 2024, 23, 2452−2473

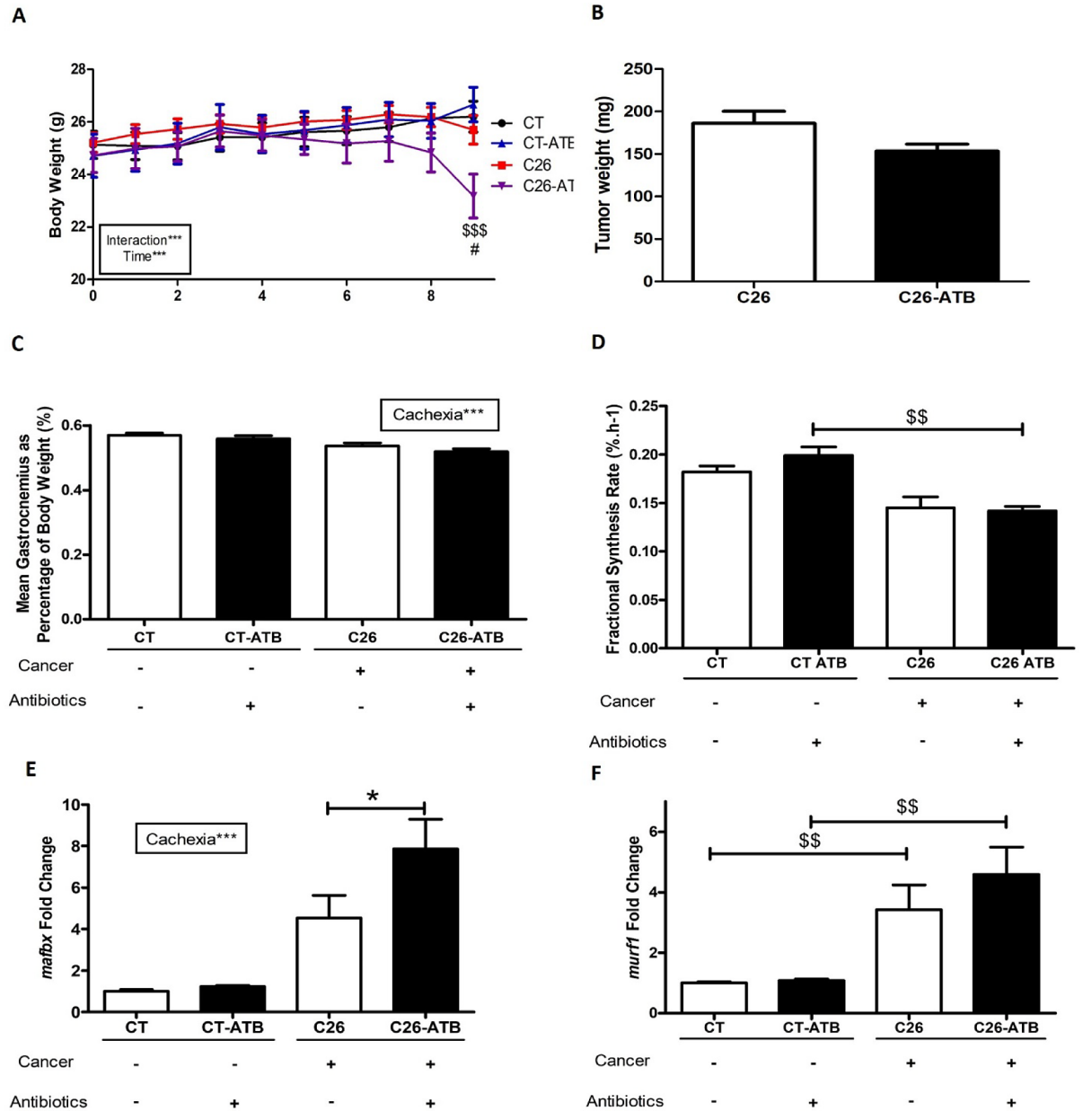

Figure 2. Impact of antibiotic treatment and cachexia on body and tumor weight and muscle characteristics. (A) Body weight evolution. Statistically significant comparisons over time between C26 and C26-ATB are shown by # and between CT-ATB and C26-ATB by $. (B) Tumor weight on the day of necropsy. (C) Gastrocnemius weight expressed as percentage of body weight on the day of necropsy, $n = 8$ mice per group. (D) Fractional synthesis rate across groups at day nine, $n = 7$ mice per group. *Mafbx* (E) and *murf1* (F) mRNA expressions in gastrocnemius muscle, $n = 8$ mice per group. CT: sham-implanted mice, CT-ATB: sham-implanted mice treated by antibiotics, C26: C26-implanted mice, C26-ATB: C26-implanted mice treated with antibiotics. Statistically significant differences between groups of figures (B)−(F) are shown with $ when Kruskal−Wallis and Dunn's post-test was used or *when a 2-way ANOVA followed by Bonferroni post-test was used. One symbol: $p < 0.05$; 2 symbols: $p < 0.01$; 3 symbols: $p < 0.001$.

9 (Figure S3) while mice treated by antibiotics presented different phyla and mouse-specific increases in different families (*Enterobacteriaceae* and *Porphyromonadaceae*). The lack of a decreased bacterial load in some mice was explained by the bloom of specific bacterial families (Figure S3), which can be due to the emergence of bacterial resistance or fungal overgrowth caused by the prolonged antibiotic treatment.[36] This confirms that despite the heterogeneous response in treated mice, gut microbiota disturbances were obtained in mice following broad-spectrum antibiotic treatment.

Effect of Cachexia and Antibiotics on Body Weight and Skeletal Muscle Mass

Initial body weight on the day of sham or C26 cell implantation (day 0) was similar across groups. There was a significant decline in body weight in C26-ATB mice, 9.5% compared to C26 mice and 13.1% compared to CT-ATB mice on day 9. Food intake was significantly decreased by 42% on day 9 between CT-ATB and C26-ATB mice (Figures 2A and S1). The tumor weight did not significantly differ between C26 and C26-ATB ($p = 0.07$, Figure 2B). Gastrocnemius and tibialis muscle weights and fiber area were similar across groups (Figures 2C and S1). In the present study, protein fractional synthesis rate in gastrocnemius

https://doi.org/10.1021/acs.jproteome.4c00143
J. Proteome Res. 2024, 23, 2452−2473

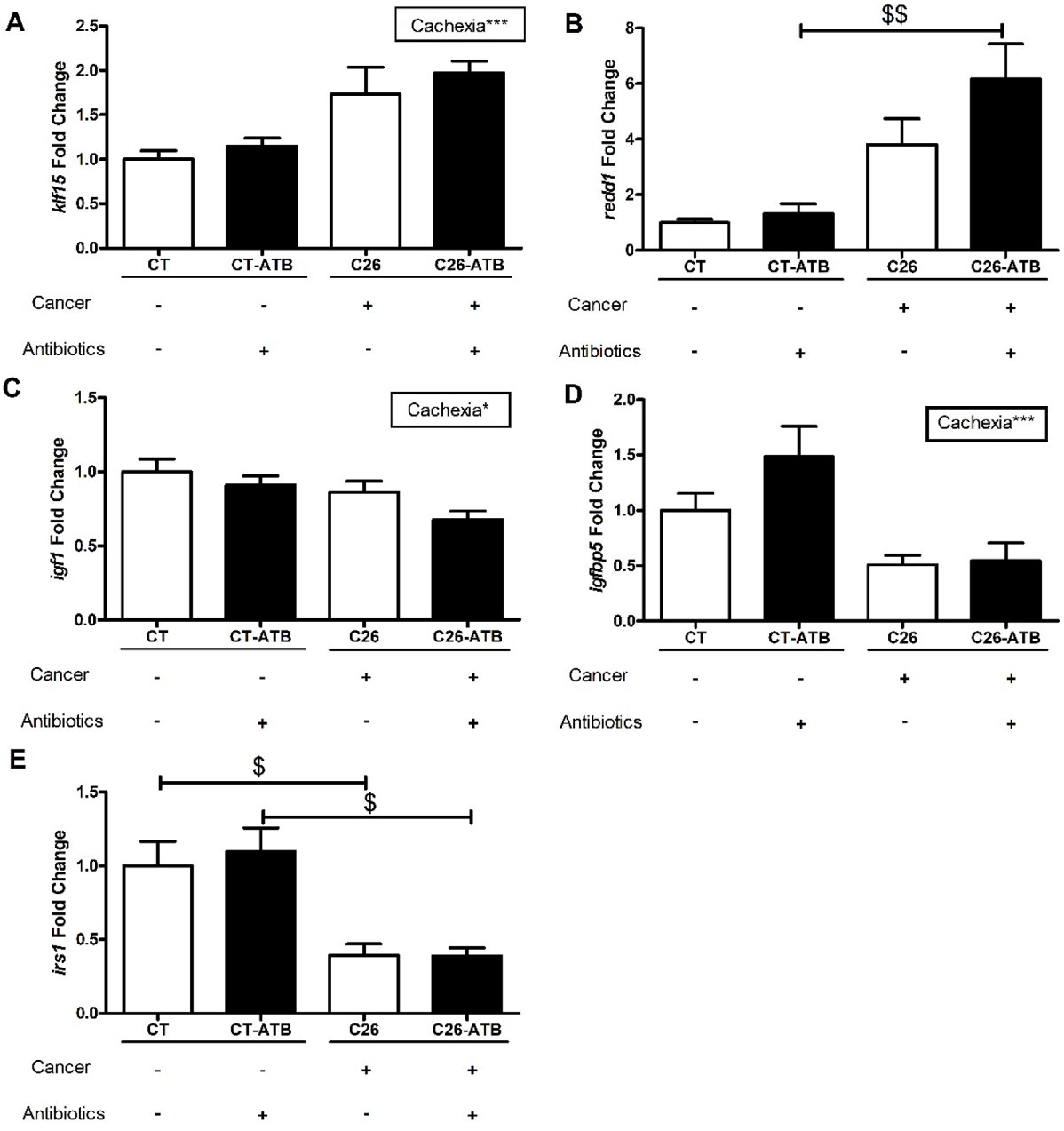

Figure 3. mRNA expressions in gastrocnemius. *Klf15* (A), *redd1* (B), *igf1* (C), *igfbp5* (D), and *irs1* (E) mRNA expressions in gastrocnemius muscle, $n = 8$ mice per group. CT: sham-implanted mice, CT-ATB: sham-implanted mice treated by antibiotics. C26: C26-implanted mice, C26-ATB: C26-implanted mice treated with antibiotics. Statistically significant differences between groups are with $ when Kruskal–Wallis and Dunn's post-test was used or * when a two-way ANOVA followed by Bonferroni post-test was used. One symbol: $p < 0.05$; 2 symbols: $p < 0.01$; 3 symbols: $p < 0.001$.

muscle was significantly decreased in C26-ATB mice compared with CT-ATB (CT-ATB: 0.19 ± 0.02%.h-1; C26-ATB: 0.14 ± 0.01), but there was no additional difference between C26 and C26-ATB mice (Figure 2D). In our experiment, *murf1* and *mafbx* gene expressions increase in mice implanted with C26 cells, by 242% versus CT mice for *murf1* and 353% for *mafbx1* compared with CT mice. Additionally, *mafbx* mRNA expression is 42.3% higher in C26-ATB mice than in C26 mice, implying an effect of both cachexia and antibiotics-induced microbial disturbances (Figures 2E,F).

mRNA expressions of the Krüppel-like factor 15 (*klf15*) and Regulated in Development and DNA Damage 1 (*redd1*) genes (Figure 3A,B) were increased in cachectic mice and more specifically in the C26-ATB group. In addition, Insulin Growth Factor 1 (*igf1*), IGF Binding Protein 5 (*igfbp5*), and Insulin receptor substrate 1 (*irs1*) gene expressions were decreased in C26 mice (Figures 3C–E). However, microbial disturbances did not induce any additional change in these mRNA expressions.

Concerning the state of cachexia, only the C26-ATB group presented a weight loss above 10%. However, the gastrocnemius relative weight was decreased as well as the muscle fractional synthesis rate in cachectic mice. Several studies have observed a decrease in gastrocnemius protein synthesis rate in C26 mice and an increase in protein degradation.[11,37] Reduced muscle protein synthesis is a known hallmark of cachexia in other preclinical models as the adenomatous polypose colon[38] mice or hepatocarcinoma mice[39] and in human patients with can-

https://doi.org/10.1021/acs.jproteome.4c00143
J. Proteome Res. 2024, 23, 2452−2473

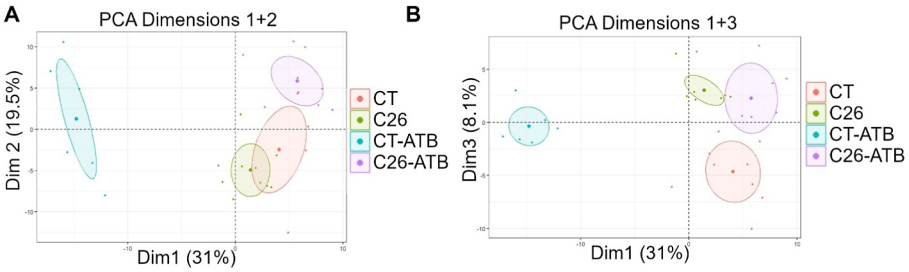

Figure 4. Principal component analyses (PCA) showing muscle proteome changes in mice with or without cachexia and with or without antibiotic treatment. PCA of all four groups showing the first two most important dimensions (A) and the first and third most important dimensions (B). CT: sham-implanted mice (n = 8), CT-ATB: sham-implanted mice treated by antibiotics (n = 6), C26: C26-implanted mice (n = 8), C26-ATB: C26-implanted mice treated with antibiotics (n = 7).

Table 2. Differentially Expressed Proteins Between the CT and C26 Groups

accession	gene	regulation	q value	unique peptides	confidence score	description	main biological process (GO)
P01027	C3	upregulated	0.001	15	1490.75187	Complement C3	GO:0045087 innate immune response
Q61646	Hp	upregulated	0.003	4	469.136376	Haptoglobin	GO:0006953 acute-phase response
Q91 × 72	Hpx	upregulated	0.005	24	2771.85141	Hemopexin	GO:0045087 innate immune response
F8VQE0	Cacna1s	upregulated	0.006	20	1888.62835	Voltage-dependent L-type calcium channel subunit alpha	GO:0030001 metal ion transport
P12246	Apcs	upregulated	0.010	3	288.060334	Serum amyloid P-component	GO:0045087 innate immune response
Q8K3 × 6	Anks4b	upregulated	0.010	2	199.853556	Ankyrin repeat and SAM domain-containing protein 4B	GO:0034976 response to endoplasmic reticulum stress
O08532	Cacna2d1	upregulated	0.010	19	2672.2766	Voltage-dependent calcium channel subunit alpha-2/delta-1	GO:0030001 metal ion transport
Q8C0M9	Asrgl1	upregulated	0.011	2	234.617686	Isoaspartyl peptidase/L-asparaginase	GO:0006530 asparagine catabolic process
D3Z2Z1	Clip1	upregulated	0.025	10	1428.45394	CAP-Gly domain-containing linker protein 1	GO:0044861 protein transport into plasma membrane raft
P19536	Cox5b	upregulated	0.035	5	560.789481	Cytochrome c oxidase subunit 5B, mitochondrial	GO:0030001 metal ion transport
Q60994	Adipoq	downregulated	0.006	3	380.32829	Adiponectin	GO:0010875 positive regulation of cholesterol efflux
B2RPU8	Zbed5	downregulated	0.010	2	163.703767	SCAN domain containing 3	No known biological process referenced

cer.[40−42] In animal models of cancer cachexia, an upregulation of genes of the catabolic[43−45] (*klf15*, *redd1*) and a downregulation of anabolic pathways[43,46] (*igf1*, *igfbp5* and *irs1*) have also been demonstrated. Overall, in this study, characteristics of a moderate state of cachexia was obtained, with a moderate body weight and skeletal muscle mass losses.

Antibiotic treatment in C26 mice induced a higher total weight loss at the end of the experiment compared with all the other groups, 9.5% compared to C26 mice, 13.1% compared to CT-ATB, and 11.5% compared to CT mice. This body weight loss was not due to a more severe disease since the tumor weight tended to decrease in the C26-ATB group. This finding of a smaller tumor has been previously described in literature, where five different models of cancer-implanted mice treated by antibiotics for 12 weeks presented a lower tumor weight than their untreated counterparts.[47] The impact of antibiotics on muscle mass in the literature is inconsistent. One study showed antibiotic treatment led to a significant decrease in rodents' skeletal muscle mass.[48] However, Nay et al.[33] obtained a lower muscle mass/total weight mass ratio in antibiotic-treated mice compared to controls, but this difference disappeared when factoring in the cecum weight change due to the antibiotic treatment.

Mafbx and *murf1* mRNA expressions are increased during cachexia preceding muscle mass loss.[49] In previous studies with microbiota interference, without cachexia, authors did not reveal changes in atrogen mRNA expression in antibiotic-treated mice.[33,48] However, the existence of different antibiotic regimes—ampicillin, streptomycin, colistin, and vancomycin—on one hand and metronidazole, on the other, makes it difficult to compare our findings. In this study, synergic effect of both microbial disturbances secondary to antibiotics and cachexia was found on the mRNA expression of *mafbx* but not *murf1*.

To conclude, our results suggest that a 14-day antibiotic treatment administered 7 days after tumor implantation to induce cachexia plays a role in altering skeletal muscle by impacting protein breakdown but not its synthesis. The significant increase of *mafbx* mRNA expression in cachectic, antibiotic-treated mice implies that microbiota influences atrogens expression.

Muscle Proteome Changes Induced by Microbial Disturbances and Cachexia

Several studies have described muscle proteome alterations induced by cancer cachexia,[13,14,16] but our study is the first to explore the proteome profile changes induced by antibiotics-

https://doi.org/10.1021/acs.jproteome.4c00143
J. Proteome Res. 2024, 23, 2452−2473

Table 3. Differentially Upregulated Proteins Between CT and CT-ATB Mice

accession	gene name	q value	unique peptides	confidence score	description	main biological process (GO)
Q99P72	Rtn4	0.000	5	998.59	reticulon-4	GO:0040007 growth; GO:0046626 regulation of insulin receptor; GO:0044861 protein transport into plasma membrane raft
D3Z2Z1	Clip1	0.000	10	1428.45	CAP-Gly domain-containing linker protein 1	GO:0044861 protein transport into plasma membrane raft; GO:0061024 membrane organization
Q02053	Uba1	0.001	29	4088.10	ubiquitin-like modifier-activating enzyme 1	GO:0006511 ubiquitin-dependent protein catabolic process
G5E8J6	Hrc	0.001	29	3482.93	histidine-rich calcium-binding protein	GO:1902081 negative regulation of calcium ion import into sarcoplasmic reticulum
Q8K010	Oplah	0.001	12	1148.62	5-oxoprolinase	GO:0006749 glutathione metabolic process
P28665	Mug1	0.001	21	2135.57	murinoglobulin-1	GO:0044703 multiorganism reproductive process
F8VPN4	Agl	0.001	20	11485.74	amylo-1,6-glucidase, 4-alpha-glucanotransferase	GO:0005980 glycogen catabolic process
A2ABU4	Myom3	0.002	4	498.26	myomesin-3	GO:0045214 sarcomere organization
P31001	Des	0.003	36	6970.73	desmin	GO:0045104 intermediate filament cytoskeleton organization
G3 × 8Q5	Cp	0.003	6	497.79	ceruloplasmin	GO:0006825 copper ion transport; GO:0006826 iron ion transport
Q14BI5	Myom2	0.007	64	21851.75	myomesin-2	GO:0045214 sarcomere organization
Q91VA7	Idh3b	0.008	2	2843.00	isocitrate dehydrogenase [NAD] subunit, mitochondrial	GO:0072350 tricarboxylic acid metabolic process
Q3U1J4	Ddb1	0.008	4	622.25	DNA damage-binding protein 1	GO:0046719 regulation by virus of viral protein levels in host cell
Q61941	Nnt	0.009	4	245.78	NAD(P) transhydrogenase, mitochondrial	GO:0042744 hydrogen peroxide catabolic process
F6RPJ9	Ide	0.009	3	421.23	insulin-degrading enzyme (fragment)	GO:0046626 regulation of insulin receptor; GO:0032092 positive regulation of protein binding
Q6P1B1	Xpnp1	0.009	2	195.05	Xaa-Pro aminopeptidase 1	GO:0043069 negative regulation of programmed cell death
Q9JMH6	Txnrd1	0.009	6	859.34	thioredoxin reductase 1, cytoplasmic	GO:0042744 hydrogen peroxide catabolic process
P47911	Rpl6	0.009	5	566.52	60S ribomal protein L6	GO:0000027 ribosomal large subunit assembly
F8VPN4	Agl	0.009	4	9633.14	4-alpha-glucanotransferase	GO:0006530 asparagine catabolic process
Q8C0M9	Asrgl1	0.010	2	234.62	isoaspartyl peptidase/L-asparaginase	GO:0036294 cellular response to decreased oxygen levels
P09411	Pgk1	0.010	71	11823.18	phphoglycerate kinase 1	GO:0005978 glycogen biosynthetic process
F6ZHD8	Gbe1	0.010	13	1833.55	1,4-alpha-glucan-branching enzyme	GO:0040007 growth
Q14BI5	Myom2	0.010	9	15863.10	myomesin-2	GO:1904106 protein localization to microvillus; GO:0034976 response to endoplasmic reticulum stress
Q64727	Vcl	0.010	23	2696.52	vinculin	GO:0040007 growth; GO:0032092 positive regulation of protein binding
Q8K3 × 6	Anks4b	0.010	2	199.85	ankyrin repeat and SAM domain-containing protein 4B	GO:0006886 intracellular protein transport
P11499	Hsp90ab1	0.011	30	5050.36	heat shock protein HSP 90-beta	GO:0044861 protein transport into plasma membrane raft; GO:0032092 positive regulation of protein binding; GO:0061024 membrane organization
E9Q1T9	Cse1l	0.011	2	363.61	exportin-2	GO:0072350 tricarboxylic acid metabolic process
Q3U2G2	Hspa4	0.011	10	1804.65	heat shock 70 kDa protein 4	GO:0045938 positive regulation of circadian sleep/wake cycle, sleep
Q99KI0	Aco2	0.012	106	17504.94	aconitate hydratase, mitochondrial	GO:0006693 prostaglandin metabolic process;GO:0033559 unsaturated fatty acid metabolic process
P07724	Alb	0.013	154	19813.85	serum albumin	GO:0007029 endoplasmic reticulum organization; GO:0061024 membrane organization
Q3TXN1	Ptgr2	0.013	2	143.35	prostaglandin reductase 2	GO:0040007 growth; GO:0046626 regulation of insulin receptor
E9Q9K5	Trdn	0.014	7	915.80	triadin	GO:0051402 neuron apoptotic process; GO:0006417 regulation of translation
Q8R146	Ah	0.014	4	300.59	acylamino-acid-releasing enzyme (Fragment)	GO:0007029 endoplasmic reticulum organization
Q8BGQ7	Aars	0.018	6	551.18	alanine–tRNA ligase, cytoplasmic	GO:0097211 cellular response to gonadotropin-releasing hormone
F8VQE0	Cacna1s	0.018	20	1888.63	voltage-dependent L-type calcium channel subunit alpha	GO:0005978 glycogen biosynthetic process
P48036	Anxa5	0.018	9	787.36	annexin A5	GO:0016567 protein ubiquitination
Q91ZJ5	Ugp2	0.019	26	3819.27	UTP–gluce-1-phphate uridylyltransferase	GO:0007029 endoplasmic reticulum organization
Q6ZQ73	Cand2	0.020	3	362.98	cullin-associated NEDD8-dissociated protein 2	GO:0061024 membrane organization
O08532	Cacna2d1	0.022	19	2672.28	voltage-dependent calcium channel subunit alpha-2/delta-1	GO:0040007 growth; GO:0006417 regulation of translation
Q78IK4	Apool	0.023	4	399.02	MIC complex subunit Mic27	GO:0030239 myofibril assembly
P52480	Pkm	0.025	125	18102.54	pyruvate kinase PKM	GO:0040007 growth
A2AMM0	Cavin4	0.026	2	194.61	caveolae-associated protein 4	GO:0010468 regulation of gene expression
P63260	Actg1	0.029	4	28499.43	actin, cytoplasmic 2	GO:0040007 growth; GO:0046626 regulation of insulin receptor; GO:0051402 neuron apoptotic process
P03921	Mtnd5	0.031	6	494.56	NADH-ubiquinone oxidoreductase chain 5	GO:0032092 positive regulation of protein binding; GO:0007029 endoplasmic reticulum organization; GO:0061024 membrane organization

https://doi.org/10.1021/acs.jproteome.4c00143
J. Proteome Res. 2024, 23, 2452−2473

Table 3. continued

accession	gene name	q value	unique peptides	confidence score	description	main biological process (GO)
Q11011	Npps	0.031	12	1613.62	puromycin-sensitive aminopeptidase	GO:0044861 protein transport into plasma membrane raft
O55143	Atp2a2	0.033	2	9063.80	sarcoplasmic/endoplasmic reticulum calcium ATPase 2	GO:0044861 protein transport into plasma membrane raft
P63017	Hspa8	0.033	55	8771.97	heat shock cognate 71 kDa protein	GO:0040007 growth; GO:0046626 regulation of insulin receptor; GO:0044861 protein transport into plasma membrane raft
P38647	Hspa9	0.034	22	2638.03	stress-70 protein, mitochondrial	GO:0032914 positive regulation of transforming growth factor beta1 production
P70670	Naca	0.038	23	2394.89	nascent polypeptide-associated complex subunit alpha, muscle-specific form	GO:0006417 regulation of translation
P51885	Lum	0.039	3	970.27	lumican	GO:0044861 protein transport into plasma membrane raft; GO:0061024 membrane organization
Q8CGC7	Eprs	0.040	8	964.19	bifunctional glutamate/proline–tRNA ligase	GO:0046626 regulation of insulin receptor; GO:0032092 positive regulation of protein binding
P48678	Lmna	0.040	16	2099.26	prelamin-A/C	GO:0046626 regulation of insulin receptor
P17182	Eno1	0.041	15	9259.44	enolase 1, alpha non-neuron	GO:0046626 regulation of insulin receptor
P29699	Ahsg	0.042	3	341.48	alpha-2-HS-glycoprotein	GO:0046626 regulation of insulin receptor; GO:0032092 positive regulation of protein binding
P05063	Aldoc	0.044	5	4163.72	aldolase C, fructose-bisphosphate	GO:0006096 glycolytic process
P48758	Cbr1	0.044	3	631.17	carbonyl reductase 1	GO:0008211 glucocorticoid metabolic process
Q6PB66	Lrpprc	0.046	7	583.86	leucine-rich PPR-motif containing	GO:0006417 regulation of translation
Q8CGK3	Lonp1	0.046	3	287.65	lon peptidase 1, mitochondrial	GO:0046626 regulation of insulin receptor
Q9EPL8	Ipo7	0.049	2	145.55	importin 7	GO:0044861 protein transport into plasma membrane raft
Q60864	Stip1	0.050	5	519.22	stress-induced phosphoprotein 1	GO:0098760 response to interleukin-7
Q8BWT1	Acaa2	0.050	25	3225.26	acetyl-coenzyme A acyltransferase 2 (mitochondrial 3-oxoacyl-coenzyme A thiolase)	GO:0061024 membrane organization; GO:0036294 cellular response to decreased oxygen levels
A2AQE4	Cops2	0.050	2	178.91	COP9 signalosome subunit 2	GO:0040007 growth

induced microbial disturbances outside and in the C26 mouse model. To better understand how microbial disturbance affects muscle metabolism in cancer cachexia, a shotgun protein analysis was performed on the gastrocnemius muscle of the CT, C26, CT-ATB, and C26-ATB mice groups. Given the wide dynamic range of protein expression in skeletal muscle, a two-step solubilization of proteins, generating a sarcoplasmic and a myofibrillar protein-enriched extract, was used from each sample. Protein quantification for each mouse was then performed by combining the myofibrillar and sarcoplasmic quantification data for each muscle.

Using this proteomic workflow, and after analyzing CT vs C26, CT vs CT-ATB, and C26 vs C26-ATB groups, 572 nonredundant proteins were identified with at least two single peptides, of which 237 proteins were differentially accumulated between groups (adjusted p value for false discovery rates below 0.05) and 209 were found to be unique.

PCA analysis uncovered a clear separation in the proteomic profile of CT-ATB and C26-ATB groups compared with those of CT and C26 groups, demonstrating a major effect of the antibiotic treatment on muscle proteome regulation (Figure 4A). Although PCA analysis showed a separation in the proteomic profile between cachectic mice (C26) and non-cachectic mice (CT), independent of the antibiotic treatment, cacaxia had a much less impact on the muscle proteome compared with the antibiotic treatment (Figure 4B).

Effect of Cachexia on the Skeletal Muscle Proteome

Regarding the effect of cachexia, we quantified only 12 differentially accumulated proteins between the CT and C26 groups (Table 2). Several studies have described skeletal muscle proteome changes induced by cancer cachexia in different models presenting a subcutaneous implantation of colon carcinoma cell lines (C26 cells), afflicted with various profiles of cachexia severity,[13,14,16] Some proteins identified in our study, such as haptoglobin, hemopexin, C3, and serum amyloid P-component, are involved in the innate immune response and are biomarkers identified in previous works.[13,16] We also found a biomarker named CACNA1S (voltage-dependent L-type calcium channel subunit alpha) that has been identified in a moderate form of cachexia.[13] This protein, expressed in skeletal muscle, is the pore-forming subunit of the dihydropyridine receptor (DHPR) and is coupled to the Ryanodine receptor Ca2+-release channel-1 (RYR1) during muscle excitation and contraction.[50] It is recognized as the cause of Dihydropyridine Receptor Congenital Myopathy.

Overall, the profile of differentially proteins that have been identified between CT and C26 mice is similar to the muscle proteome in mice with moderate cachexia and minor muscle mass weight losses.[13,16]

Effect of Microbial Disturbances—Induced by Antibiotic Treatment on the Skeletal Muscle Proteome

We focused on the effect of microbial disturbances induced by antibiotics on the skeletal muscle proteome, independent of cachexia, since antibiotic treatment induced a major effect on the muscle proteome expression. First, looking at the differentially accumulated proteins between the CT and CT-ATB groups, 143 differentially proteins were found, with 62 upregulated and 81 downregulated proteins (Tables 3 and 4). Then we focused on the pathways involved in the proteome changes.

Impact on Skeletal Muscle Metabolism. To identify the relevant biological processes (BP) involved in the muscle proteome changes observed in the CT-ATB group, a Gene Ontology (GO) analysis was performed on the proteins with an increased differential expression and a lowered differential expression in the gastrocnemius muscle. The most over-represented GO_BP terms for the proteins with increased

https://doi.org/10.1021/acs.jproteome.4c00143
J. Proteome Res. 2024, 23, 2452−2473

Table 4. Differentially Down-Regulated Proteins Between CT and CT-ATB Mice

accession	gene Name	q value	unique peptides	confidence score	description	main biological process
B2RPU8	Zbed5	<0.001	2	163.70	SCAN domain containing 3	no known biological process referenced
D3YUK4	Ndufb10	<0.001	6	567.20	NADH dehydrogenase [ubiquinone] 1 beta subcomplex subunit 10 (Fragment)	GO:0042776 proton motive force-driven mitochondrial ATP synthesis
Q9D6J6	Ndufv2	<0.001	3	381.07	NADH dehydrogenase [ubiquinone] flavoprotein 2, mitochondrial	GO:0042776 proton motive force-driven mitochondrial ATP synthesis
Q9D172	Gatd3a	<0.001	9	1040.48	glutamine amidotransferase-like class 1 domain-containing protein 3A, mitochondrial	no known biological process referenced
Q91VB8	Hba-a1	0.001	4	2408.84	alpha globin 1	GO:0030099 myeloid cell differentiation
P14206	Rpsa	0.001	3	323.57	40S ribomal protein SA	GO:0042255 ribosome assembly
P01942	Hba	0.001	8	2699.03	hemoglobin subunit alpha	no known biological process referenced
P05977	Myl1	0.001	69	22956.43	myin light chain 1/3, skeletal muscle isoform	GO:0060048 cardiac muscle contraction
Q99LY9	Ndufs5	0.001	4	215.31	NADH dehydrogenase [ubiquinone] iron−sulfur protein 5	GO:0042776 proton motive force-driven mitochondrial nthesis
O88342	Wdr1	0.002	3	460.25	WD repeat-containing protein 1	GO:0030099 myeloid cell differentiation; GO:0043243 positive regulation of protein-containing complex disassembly
Q9D1G3	Hhatl	0.003	7	799.49	protein-cysteine N-palmitoyltransferase HHAT-like protein	GO:1903060 negative regulation of protein lipidation
Q922B1	Macrod1	0.003	7	844.25	ADP-ribe glycohydrolase MACROD1	GO:0042278 purine nucleoside metabolic process
P63028	Tpt1	0.003	4	390.12	translationally controlled tumor protein	GO:1902230 negative regulation of intrinsic apoptotic signaling pathway in response to DNA damage
P09542	Myl3	0.003	5	3910.69	myin light chain 3	GO:0060048 cardiac muscle contraction
P20108	Prdx3	0.003	4	569.80	thioredoxin-dependent peroxide reductase, mitochondrial	GO:0042776 proton motive force-driven mitochondrial ATP synthesis; GO:0030099 myeloid cell differentiation
Q5EBG6	Hspb6	0.003	2	275.03	heat shock protein beta-6	GO:0010664 negative regulation of striated muscle cell apoptotic process
P97457	Mylpf	0.003	41	15699.02	myin regulatory light chain 2, skeletal muscle isoform	GO:0006936 muscle contraction
P02088	Hbb-b1	0.003	11	5054.03	hemoglobin subunit beta-1	GO:0030099 myeloid cell differentiation
Q9CQC7	Ndufb4	0.003	2	172.49	NADH dehydrogenase [ubiquinone] 1 beta subcomplex subunit 4	GO:0042776 proton motive force-driven mitochondrial ATP synthesis
Q8BVJ7	Pdlim7	0.004	11	1541.87	PDZ and LIM domain protein 7	GO:0001503 ossification
P31786	Dbi	0.005	2	200.39	acyl-CoA-binding protein	GO:1905952 regulation of lipid localization
P53996	Cnbp	0.007	3	282.20	cellular nucleic acid-binding protein	GO:2000765 regulation of cytoplasmic translation
Q91YE8	Synpo2	0.007	6	3490.69	synaptopodin-2	GO:0043243 positive regulation of protein-containing complex disassembly
Q64433	Hs1	0.007	2	287.43	10 kDa heat shock protein, mitochondrial	GO:0051085 chaperone cofactor-dependent protein refolding
P63242	Eif5a	0.008	4	473.38	eukaryotic translation initiation factor 5A−1	GO:0043243 positive regulation of protein-containing complex disassembly
P02089	Hbb-b2	0.009	9	3872.23	hemoglobin subunit beta-2	GO:0030099 myeloid cell differentiation
Q9CQJ8	Ndufb9	0.009	9	805.44	NADH dehydrogenase [ubiquinone] 1 beta subcomplex subunit 9	GO:0042776 proton motive force-driven mitochondrial ATP synthesis
Q9D855	Uqcrb	0.009	6	643.25	cytochrome *b*-c1 complex subunit 7	GO:0042776 proton motive force-driven mitochondrial ATP synthesis
Q00623	Apoa1	0.009	4	318.66	apolipoprotein A-I	GO:0042776 proton motive force-driven mitochondrial ATP synthesis; GO:1905952 regulation of lipid localization
Q60994	Adipoq	0.009	3	380.33	adiponectin	GO:1905952 regulation of lipid localization
P56391	Cox6b1	0.009	7	1012.82	cytochrome c oxidase subunit 6B1	GO:0006123 mitochondrial electron transport
Q91 V79	Fitm1	0.009	2	175.97	fat storage-inducing transmembrane protein 1	GO:0042776 proton motive force-driven mitochondrial ATP synthesis; GO:1905952 regulation of lipid localization
Q9R059	Fhl3	0.009	7	899.35	four-and-a-half LIM domains protein 3	GO:0030036 actin cytoskeleton organization

https://doi.org/10.1021/acs.jproteome.4c00143
J. Proteome Res. 2024, 23, 2452−2473

Table 4. continued

accession	gene Name	q value	unique peptides	confidence score	description	main biological process
O88569	Hnrnpa2b1	0.010	4	589.27	heterogeneous nuclear ribonucleoproteins A2/B1	GO:0043243 positive regulation of protein-containing complex disassembly; GO:0016071 mRNA metabolic process
P43023	Cox6a2	0.010	2	264.84	cytochrome c oxidase subunit 6A2, mitochondrial	GO:0042776 proton motive force-driven mitochondrial ATP synthesis
Q99MR8	Mccc1	0.011	2	308.01	methylcrotonoyl-CoA carboxylase subunit alpha, mitochondrial	GO:0006552 leucine catabolic process
Q9CR68	Uqcrfs1	0.012	8	1500.55	cytochrome *b*-c1 complex subunit Rieske, mitochondrial	GO:0042776 proton motive force-driven mitochondrial ATP synthesis
P99028	Uqcrh	0.013	4	273.23	cytochrome *b*-c1 complex subunit 6, mitochondrial	GO:0042776 proton motive force-driven mitochondrial ATP synthesis
P14869	Rplp0	0.013	3	380.50	60S acidic ribomal protein P0	GO:0070670 response to interleukin-4
J3QP56	Lypla1	0.014	3	225.67	acyl-protein thioesterase 1	GO:0002084 protein depalmitoylation
Q9DCX2	Atp5pd	0.014	17	2312.64	ATP synthase subunit d, mitochondrial	GO:0042776 proton motive force-driven mitochondrial ATP synthesis
Q9CQH3	Ndufb5	0.015	4	410.63	NADH dehydrogenase [ubiquinone] 1 beta subcomplex subunit 5, mitochondrial	GO:0042776 proton motive force-driven mitochondrial ATP synthesis
P19157	Gstp1	0.016	14	1607.29	glutathione S-transferase P 1	GO:1905952 regulation of lipid localization
E9PYJ9	Ldb3	0.017	101	11819.49	LIM domain-binding protein 3	GO:0045214 sarcomere organization
P13541	Myh3	0.018	14	29881.57	myin-3	GO:0042776 proton motive force-driven mitochondrial ATP synthesis; GO:0003009 skeletal muscle contraction
P20801	Tnnc2	0.018	15	2043.29	troponin C, skeletal muscle	GO:0003009 skeletal muscle contraction
Q9DCJ5	Ndufa8	0.019	10	1183.89	NADH dehydrogenase [ubiquinone] 1 alpha subcomplex subunit 8	GO:0042776 proton motive force-driven mitochondrial ATP synthesis
Q9CR61	Ndufb7	0.019	4	383.18	NADH dehydrogenase [ubiquinone] 1 beta subcomplex subunit 7	GO:0042776 proton motive force-driven mitochondrial ATP synthesis
Q8K4Z3	Naxe	0.020	3	388.30	NAD(P)H-hydrate epimerase	GO:1905952 regulation of lipid localization
P49813	Tmod1	0.020	6	1076.18	tropomodulin-1	GO:0051694 pointed-end actin filament capping
Q8BH95	Echs1	0.020	4	421.65	Enoyl-CoA hydratase, mitochondrial	GO:0006635 fatty acid beta-oxidation
Q8K3J1	Ndufs8	0.021	3	757.29	NADH dehydrogenase [ubiquinone] iron−sulfur protein 8, mitochondrial	GO:0042776 proton motive force-driven mitochondrial ATP synthesis
P14602	Hspb1	0.025	4	431.85	heat shock protein beta-1	GO:1905952 regulation of lipid localization
P42125	Eci1	0.025	8	803.99	Enoyl-CoA delta isomerase 1, mitochondrial	GO:0006635 fatty acid beta-oxidation
P47857	Pfkm	0.025	96	13321.74	ATP-dependent 6-phphofructokinase, muscle type	GO:0030388 fructose 1,6-bisphosphate metabolic process
P61027	Rab10	0.026	2	237.33	Ras-related protein Rab-10	GO:0097051 establishment of protein localization to endoplasmic reticulum membrane
P97443	Smyd1	0.026	23	2976.66	histone-lysine *N*-methyltransferase Smyd1	GO:0010830 regulation of myotube differentiation
P16858	Gapdh	0.026	2	14128.13	glyceraldehyde-3-phphate dehydrogenase	GO:1905952 regulation of lipid localization
Q99LC3	Ndufa10	0.026	11	1838.41	NADH dehydrogenase [ubiquinone] 1 alpha subcomplex subunit 10, mitochondrial	GO:0042776 proton motive force-driven mitochondrial ATP synthesis
A8JYK8	Ephx2	0.028	2	238.55	bifunctional epoxide hydrolase 2	GO:0002539 prostaglandin production involved in inflammatory response
P45591	Cfl2	0.029	6	976.27	cofilin-2	GO:0043243 positive regulation of protein-containing complex disassembly
P57776	Eef1d	0.029	3	383.70	elongation factor 1-delta	GO:0016071 mRNA metabolic process
E9PWG4	Myl1	0.031	6	13312.55	myin light chain 1/3, skeletal muscle isoform	GO:1905952 regulation of lipid localization
P62631	Eef1a2	0.034	25	4831.36	elongation factor 1-alpha 2	GO:0007155 cell adhesion
P70402	Mybph	0.035	13	1602.66	myin-binding protein H	GO:0016071 mRNA metabolic process
Q9WV35	Apobec2	0.036	10	1193.36	C→U-editing enzyme APOBEC-2	GO:0042776 proton motive force-driven mitochondrial ATP synthesis
P70404	Idh3g	0.037	22	3260.89	isocitrate dehydrogenase [NAD] subunit gamma 1, mitochondrial	GO:0042776 proton motive force-driven mitochondrial ATP synthesis; GO:1905952 regulation of lipid localization
P97450	Atp5pf	0.039	4	317.90	ATP synthase-coupling factor 6, mitochondrial	GO:0006635 fatty acid beta-oxidation
Q9CQ62	Decr1	0.039	6	507.87	2,4-dienoyl-CoA reductase, mitochondrial	GO:0003009 skeletal muscle contraction

https://doi.org/10.1021/acs.jproteome.4c00143
J. Proteome Res. 2024, 23, 2452−2473

Table 4. continued

accession	gene Name	q value	unique peptides	confidence score	description	main biological process
E9PVN9	Tnnt3	0.039	2	10424.46	troponin T, fast skeletal muscle	GO:0016071 mRNA metabolic process
Q8BG05	Hnrnpa3	0.040	3	219.17	heterogeneous nuclear ribonucleoprotein A3	GO:0042776 proton motive force-driven mitochondrial ATP synthesis
Q9D6J5	Ndufb8	0.040	5	424.12	NADH dehydrogenase [ubiquinone] 1 beta subcomplex subunit 8, mitochondrial	GO:0042776 proton motive force-driven mitochondrial ATP synthesis: GO:0043243 positive regulation of protein-containing complex disassembly
Q60932	Vdac1	0.043	8	4953.16	voltage-dependent anion-selective channel protein 1	GO:0043161 proteasome-mediated ubiquitin-dependent protein catabolic process
O55234	Psmb5	0.044	2	217.57	proteasome subunit beta type-5	GO:0042776 proton motive force-driven mitochondrial ATP synthesis
Q9DC69	Ndufa9	0.044	17	2178.83	NADH dehydrogenase [ubiquinone] 1 alpha subcomplex subunit 9, mitochondrial	GO:0043243 positive regulation of protein-containing complex disassembly
Q9JJV2	Pfn2	0.044	3	313.04	profilin-2	GO:0007015 actin filament organization
O70209	Pdlim3		8	807.22	PDZ and LIM domain protein 3	GO:0030099 myeloid cell differentiation
P04247	Mb		70	10193.13	myoglobin	GO:0003009 skeletal muscle contraction
Q3MI48	Jsrp1		5	401.67	junctional sarcoplasmic reticulum protein 1	GO:0042776 proton motive force-driven mitochondrial ATP synthesis
Q9CQQ7	Atp5pb		15	1974.33	ATP synthase F(0) complex subunit B1, mitochondrial	GO:0042776 proton motive force-driven mitochondrial ATP synthesis
Q99KQ4	Nampt		9	1076.13	nicotinamide phosphoribosyltransferase	GO:0042776 proton motive force-driven mitochondrial ATP synthesis

expression were "growth", "regulation of insulin receptor pathway", and "intracellular protein transport" (Figure 5A). Previous papers interested in the muscle of germ-free mice[43] and mice treated with antibiotics then reseeded[33] have also identified modifications on these biological processes, notably growth via the insulin growth factor pathways that imply the expression of IGF1,[33,43] IGFBP3, and IGFBP5[43]. Speaking of the insulin receptor pathway, bacterial extracellular vesicles extracted from the stools of mice fed a high fat diet have been administered to mice and can induce insulin resistance in mice as well as be traced back to the skeletal muscle.[51] Thus, the increased differentially expressed proteins implicated in the regulation of growth and insulin receptor pathway of our CT-ATB mice could reflect that glucose metabolism alterations are induced by microbial disturbances in our model.

The most overrepresented GO-BP terms for the proteins that displayed a lower expression in CT-ATB mice compared with CT mice were "mitochondrial ATP synthesis", "myeloid cell differentiation", and "regulation of lipid localization" (Figure 5A). Protein−protein interactions also identified a cluster implicated in "oxidative phosphorylation" (Figure 5D,E). Some authors have also observed that germ-free mice, whichpresent a lower fat mass than conventionalized mice,[52] display increased activity of proteins responsible for fatty acid oxidation, such as AMPK,[43] ACACA or AcetylCoA carboxylase and CPT1, carnitine:palmitoyl transferase-1,[53] as well as reduced gene expression of the components of the mitochondrial respiratory chain.[43] In animal models with antibiotic treatments, piglets fed antibiotics long-term by tylosin phosphate also develop an increased expression of genes involved in lipid accumulation in muscle: *acetylcoa carboxylase* and *lipoprotein lipase*.[54] In mice, low doses of penicillin also lead to downplayed gene expression of mitochondrial electron transport components.[43] Finally, directly administering microbial byproducts such as short chain fatty acids to germ-free mice also improves skeletal muscle weight, mRNA *mafbx1* expression and grip strength.[43] This suggests a link between the microbiota and energy metabolism at the lipid and mitochondrial level that might affect skeletal muscle performances.

Overall, our results and previous literature suggest an upstream impact of microbiota on mitochondrial muscle energy metabolism and lipid localization.

Impact on Skeletal Muscle Function. Interestingly, the GO-BP term "skeletal muscle contraction" was downregulated (Figure 5A). In addition, protein−protein interaction analyses (Figure 5D,E) highlighted that clusters involved "muscle contraction" and "actin cytoskeleton organization". Although mechanisms are not clearly described, several studies have demonstrated a link between gut microbiota and skeletal muscle regulation. Indeed, in mice treated with antibiotics, the relative muscle weight and *ex vivo* muscle fatigue alterations were reversed by reseeding.[33] Moreover, supplementing mice with *Lactobacillus plantarum* leads to increased muscle function in a dose-dependent way.[55] In humans, supplementing triathlon sportsmen over two months with *Lactobacillus plantarum* improved the fatigue index and maximum O_2 volume after a triathlon performance.[56] Our results revealed a cluster of four proteins involved in the actin filament composition: FHL3 (four and a half LIM domains protein 3), PDLIM 3, 6, and 7 (PDZ and LIM domain proteins 3, 6 and 7). These proteins are interesting targets in skeletal muscle because their mutations can lead to myopathies. They contribute to satellite cell differentiation, muscle fiber stress response, and are at the center of

https://doi.org/10.1021/acs.jproteome.4c00143
J. Proteome Res. 2024, 23, 2452−2473

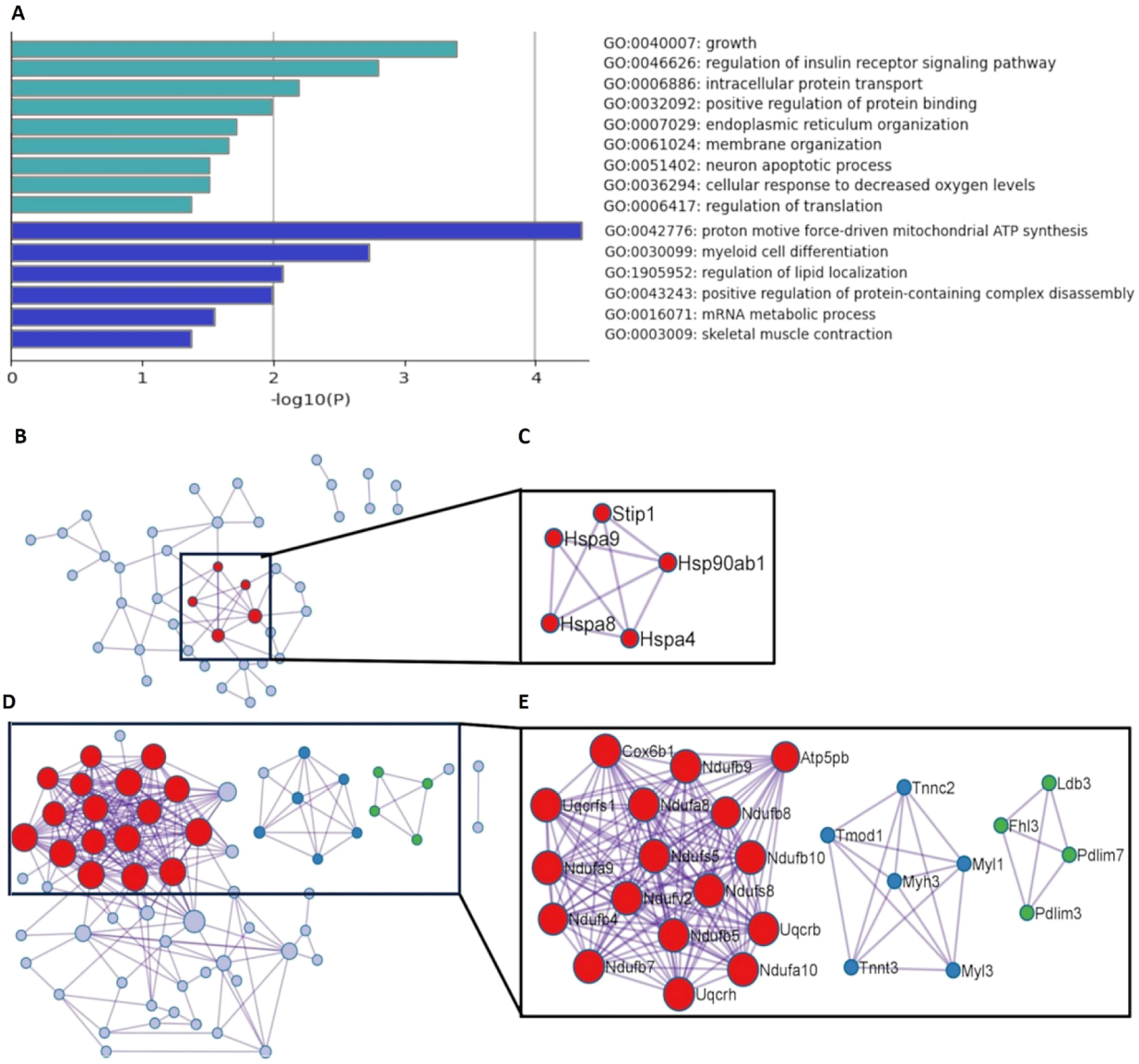

Figure 5. Proteome changes in the gastrocnemius of mice without cachexia, treated by antibiotics. (A) Biological processes differentially expressed with a higher expression (green) or a lower expression (blue) of proteins for CT-ATB mice compared with the CT group. Protein−protein interactions between CT and CT-ATB groups within the positively differentially expressed proteins (B) with a focus on one protein cluster (C). Protein−protein interactions between CT and CT-ATB groups within the negatively expressed proteins (D) with a focus on three protein clusters (E). Red nodes correspond to proteins involved in protein folding in figure C, and oxidative phosphorylation corresponds to proteins involved in muscle contractions, and green nodes correspond to proteins involved in actin cytoskeleton organization. CT: sham-implanted mice (n = 8), CT-ATB: sham-implanted mice treated by antibiotics (n = 6).

the Z disc−actin−cytoskeleton interaction.[57] In particular, PDLIM6 KO mice display cardiomyopathy with lowered survival and altered skeletal muscle sarcomere organization at the Z line after birth.[58,59] Altogether, these proteins with LIM domains and PDZ domains seem specifically expressed during muscle remodeling in response to microbial disturbances and, thus, represent potential biomarkers.

Impact on Protein Folding. Protein−protein interaction analyses also revealed a cluster of positively, differentially expressed proteins involved in "protein folding" (Figure 5B,C), with the identification of STIP1 (stress-induced phosphoprotein 1) and HSPs (Heat shock proteins) of the HSP70/HSP family: a4, a8, a9, and the HSP90/C family: 90ab1.[60] HSPs are major players of efficient protein folding, or if not attained, autophagy of misfolded proteins.[61] Their mutations lead to myopathies in human patients.[62] Heat stress will lead to the induction of anabolic pathways such as the Akt/mTOR pathway,[63] while HSP70 overexpression can revert the mRNA overexpression of *murf1* and *mafbx* via *foxo3*.[64] Among the HSPs identified in our study, HSPa4 is part of the HSP70 family, and HSPa4 knockout mice present significant skeletal muscle mass loss, a higher muscle inflammatory cell presence, greater fiber degeneration, and impaired autophagy and apoptosis processes.[61] This family of proteins thus seems an interesting choice to explore the link between skeletal muscle and microbiota outside of cachexia.

This is the first analysis, to our knowledge, investigating the impact of microbiota modulation by antibiotics on the skeletal muscle proteome. Overall, the changes in the muscle proteome of mice due to microbial disturbances secondary to antibiotic treatment explained the majority of the proteome variation seen

https://doi.org/10.1021/acs.jproteome.4c00143
J. Proteome Res. 2024, 23, 2452−2473

Table 5. Differentially Expressed Proteins between the C26 and C26-ATB Groups

accession	gene Name	regulation	q value	unique peptides	confidence score	Description	main biological processes
P97450	Atp5pf	downregulated	0.017	4	317.90	ATP synthase-coupling factor 6, mitochondrial	GO:0032307 negative regulation of prostaglandin secretion
A2AKU9	Atp5c1	downregulated	0.018	4	1308.71	ATP synthase subunit gamma	GO:0042776 proton motive force-driven mitochondrial ATP synthesis
P19536	Cox5b	downregulated	0.020	5	560.79	Cytochrome c oxidase subunit 5B, mitochondrial	GO:0042775 mitochondrial ATP synthesis coupled electron transport
O55143	Atp2a2	downregulated	0.028	2	9063.80	Sarcoplasmic/endoplasmic reticulum calcium ATPase 2	GO:1903515 calcium ion transport from cytosol to endoplasmic reticulum
Q64737	Gart	upregulated	0.002	7	846.32	Trifunctional purine biosynthetic protein adenosine-3	GO:0010035 response to inorganic substance
Q91ZJ5	Ugp2	upregulated	0.005	26	3819.27	UTP–glucose-1-phosphate uridylyltransferase	GO:0006006 glucose metabolic process
E9Q1T9	Cse1l	upregulated	0.006	2	363.61	Exportin-2	GO:0072350 tricarboxylic acid metabolic process
P14152	Mdh1	upregulated	0.006	22	3360.34	Malate dehydrogenase, cytoplasmic	GO:0006006 glucose metabolic process; GO:0006739 NADP metabolic process
Q93092	Taldo1	upregulated	0.007	4	375.69	Transaldolase	GO:0006006 glucose metabolic process; GO:1901615 organic hydroxy compound metabolic process; GO:0006739 NADP metabolic process
Q9EPL8	Ipo7	upregulated	0.008	2	145.55	Importin-7	GO:0044861 protein transport into plasma membrane raft
P05132	Prkaca	upregulated	0.011	8	762.80	cAMP-dependent protein kinase catalytic subunit alpha	GO:0007369 gastrulation; GO:0048729 tissue morphogenesis; GO:0009743 response to carbohydrate; GO:0062013 positive regulation of small molecule metabolic process
H3BL49	Cct8	upregulated	0.011	2	111.49	T-complex protein 1 subunit theta	GO:0009410 response to xenobiotic stimulus; GO:0051052 regulation of DNA metabolic process
Q9R062	Gyg1	upregulated	0.011	12	1357.37	Glycogenin-1	GO:0006006 glucose metabolic process
O08911	Mapk12	upregulated	0.011	3	682.81	Mitogen-activated protein kinase 12	GO:0000165 MAPK cascade
P35486	Pdha1	upregulated	0.011	47	5404.38	Pyruvate dehydrogenase E1 component subunit alpha, somatic form, mitochondrial	GO:0006006 glucose metabolic process
Q8BZA9	Tigar	upregulated	0.011	2	295.57	Fructose-2,6-bisphosphatase TIGAR	GO:0006006 glucose metabolic process; GO:0009410 response to xenobiotic stimulus; GO:1901615 organic hydroxy compound metabolic process; GO:0009743 response to carbohydrate; GO:0000902 cell morphogenesis; GO:0050900 leukocyte migration
B0QZL1	Eno1	upregulated	0.014	2	3483.28	2-phospho-D-glycerate hydro-lyase (Fragment)	GO:0006006 glucose metabolic process; GO:0062013 positive regulation of small molecule metabolic process
E9Q8K5	Ttn	upregulated	0.016	96	16695.77	Titin	GO:0009410 response to xenobiotic stimulus; GO:0048729 tissue morphogenesis; GO:0050900 leukocyte migration; GO:0040007 growth
Q3U1J4	Ddb1	upregulated	0.018	4	622.25	DNA damage-binding protein 1	GO:0062013 positive regulation of small molecule metabolic process
Q11011	Npps	upregulated	0.018	12	1613.62	Puromycin-sensitive aminopeptidase	GO:0007369 gastrulation; GO:0006006 glucose metabolic process; GO:0009410 response to xenobiotic stimulus; GO:1901615 organic hydroxy compound metabolic process; GO:0048729 tissue morphogenesis; GO:0050900 leukocyte migration; GO:0040007 growth
Q91XH5	Spr	upregulated	0.018	5	691.84	Sepiapterin reductase	GO:0006006 glucose metabolic process; GO:1901615 organic hydroxy compound metabolic process; GO:0000902 cell morphogenesis
P00329	Adh1	upregulated	0.019	2	739.69	Alcohol dehydrogenase 1	GO:0006006 glucose metabolic process; GO:1901615 organic hydroxy compound metabolic process; GO:0048729 tissue morphogenesis; GO:0009743 response to carbohydrate
Q80UY1	Carnmt1	upregulated	0.020	6	481.83	Carnosine *N*-methyltransferase	GO:0035498 carnosine metabolic process
Q9CPU0	Glo1	upregulated	0.020	11	1709.74	Lactoylglutathione lyase	GO:0006006 glucose metabolic process; GO:1901615 organic hydroxy compound metabolic process; GO:0048729 tissue morphogenesis; GO:0006089 lactate metabolic process
Q8CG76	Akr7a2	upregulated	0.024	2	267.41	Aflatoxin B1 aldehyde reductase member 2	GO:0006629 lipid metabolic process
P70296	Pepbp1	upregulated	0.024	11	1214.49	Phosphatidylethanolamine-binding protein 1	GO:0043409 negative regulation of MAPK cascade

https://doi.org/10.1021/acs.jproteome.4c00143
J. Proteome Res. 2024, 23, 2452−2473

Table 5. continued

accession	gene Name	regulation	q value	unique peptides	confidence score	Description	main biological processes
P24527	Lta4h	upregulated	0.024	7	823.19	Leukotriene A-4 hydrolase	GO:0006006 glucose metabolic process
O55234	Psmb5	upregulated	0.024	2	217.57	Proteasome subunit beta type-5	GO:0043161 proteasome-mediated ubiquitin-dependent protein catabolic process
Q3TLP8	Rac1	upregulated	0.024	3	351.38	Ras-related C3 botulinum toxin substrate 1	GO:0007369 gastrulation; GO:0009410 response to xenobiotic stimulus; GO:0048729 tissue morphogenesis; GO:0009743 response to carbohydrate; GO:0007264 small GTPase mediated signal transduction; GO:0050900 leukocyte migration; GO:0051052 regulation of DNA metabolic process
O88342	Wdr1	upregulated	0.024	3	460.25	WD repeat-containing protein 1	GO:0048729 tissue morphogenesis; GO:0000902 cell morphogenesis; GO:0050900 leukocyte migration
Q99PT1	Arhgdia	upregulated	0.026	5	616.05	Rho GDP-dissociation inhibitor 1	GO:0007264 small GTPase mediated signal transduction; GO:0050900 leukocyte migration
Q9ET80	Jph1	upregulated	0.027	8	785.99	Junctophilin-1	GO:0007517 muscle organ development
P28474	Adh5	upregulated	0.028	9	1284.33	Alcohol dehydrogenase class-3	GO:0006006 glucose metabolic process; GO:0009410 response to xenobiotic stimulus; GO:1901615 organic hydroxy compound metabolic process; GO:0000902 cell morphogenesis
P45591	Cfl2	upregulated	0.028	6	976.27	Cofilin-2	GO:0050900 leukocyte migration
Q6P8J7	Ckmt2	upregulated	0.028	60	9652.68	Creatine kinase S-type, mitochondrial	GO:0006603 phosphocreatine metabolic process
P06745	Gpi	upregulated	0.028	55	10092.28	Glucose-6-phosphate isomerase	GO:0007369 gastrulation; GO:0006006 glucose metabolic process; GO:0048729 tissue morphogenesis; GO:0009743 response to carbohydrate
P06151	Ldha	upregulated	0.028	60	13993.69	L-lactate dehydrogenase A chain	GO:0006006 glucose metabolic process; GO:1901615 organic hydroxy compound metabolic process; GO:0006089 lactate metabolic process; GO:0006739 NADP metabolic process
Q9D6J6	Ndufv2	upregulated	0.028	3	381.07	NADH dehydrogenase [ubiquinone] flavoprotein 2, mitochondrial	GO:0042776 proton motive force-driven mitochondrial ATP synthesis
P10518	Alad	upregulated	0.030	2	121.06	Delta-aminolevulinic acid dehydratase	GO:0009410 response to xenobiotic stimulus; GO:0010035 response to inorganic substance
Q99M71	Epdr1	upregulated	0.030	3	423.72	Mammalian ependymin-related protein 1	GO:0007264 small GTPase mediated signal transduction
Q9DCL9	Paics	upregulated	0.030	3	266.07	Multifunctional protein ADE2	GO:0044208'de novo' AMP biosynthetic process
Q9D8N0	Eef1g	upregulated	0.031	8	1110.49	Elongation factor 1-gamma	GO:0006412 translation
Q9CZD3	Gars1	upregulated	0.031	8	1075.43	Glycine–tRNA ligase	GO:0070150 mitochondrial glycyl-tRNA aminoacylation
O08749	Dld	upregulated	0.033	24	3877.22	Dihydrolipoyl dehydrogenase, mitochondrial	GO:0007369 gastrulation; GO:0006006 glucose metabolic process; GO:0048729 tissue morphogenesis
O70250	Pgam2	upregulated	0.033	57	9715.02	Phosphoglycerate mutase 2	GO:0006006 glucose metabolic process; GO:0010035 response to inorganic substance
P54071	Idh2	upregulated	0.033	23	3174.77	Isocitrate dehydrogenase [NADP], mitochondrial	GO:0006006 glucose metabolic process; GO:0009410 response to xenobiotic stimulus; GO:1901615 organic hydroxy compound metabolic process; GO:0007264 small GTPase mediated signal transduction; GO:0006739 NADP metabolic process
P26883	Fkbp1a	upregulated	0.036	5	402.33	Peptidyl-prolyl cis−trans isomerase FKBP1A	GO:0048729 tissue morphogenesis
Q3MI48	Jsrp1	upregulated	0.036	5	401.67	Junctional sarcoplasmic reticulum protein 1	GO:0003009 skeletal muscle contraction
P16125	Ldhb	upregulated	0.036	15	2829.90	L-lactate dehydrogenase B chain	GO:0006006 glucose metabolic process; GO:1901615 organic hydroxy compound metabolic process; GO:0006089 lactate metabolic process; GO:0006739 NADP metabolic process
P61089	Ube2n	upregulated	0.036	2	199.97	Ubiquitin-conjugating enzyme E2 N	GO:0009410 response to xenobiotic stimulus; GO:0000902 cell morphogenesis; GO:0051052 regulation of DNA metabolic process
Q60994	Adipoq	upregulated	0.036	3	380.33	Adiponectin	GO:0006006 glucose metabolic process; GO:0009410 response to xenobiotic stimulus; GO:0048729 tissue morphogenesis; GO:0009743 response to carbohydrate; GO:0000902 cell morphogenesis; GO:0007264 small GTPase mediated signal transduction; GO:0051052 regulation of DNA metabolic process
Q61598	Gdi2	upregulated	0.036	7	1647.70	Rab GDP dissociation inhibitor beta	GO:0007264 small GTPase mediated signal transduction
Q3THS6	Mat2a	upregulated	0.036	2	283.50	S-adenosylmethionine synthase	GO:0009410 response to xenobiotic stimulus; GO:0048729 tissue morphogenesis; GO:0009743 response to carbohydrate

https://doi.org/10.1021/acs.jproteome.4c00143
J. Proteome Res. 2024, 23, 2452−2473

Table 5. continued

accession	gene Name	regulation	q value	unique peptides	confidence score	Description	main biological processes
Q8R016	Blmh	upregulated	0.038	2	338.32	Bleomycin hydrolase	GO:0006006 glucose metabolic process; GO:0009410 response to xenobiotic stimulus
P10126	Eef1a1	upregulated	0.038	2	1970.43	Elongation factor 1-alpha 1	GO:0009410 response to xenobiotic stimulus
P19157	Gstp1	upregulated	0.038	14	1607.29	Glutathione S-transferase P 1	GO:0006006 glucose metabolic process; GO:0009410 response to xenobiotic stimulus; GO:0007264 small GTPase mediated signal transduction; GO:0006089 lactate metabolic process
P31938	Map2k1	upregulated	0.038	2	160.39	Dual specificity mitogen-activated protein kinase kinase 1	GO:0007369 gastrulation; GO:0009410 response to xenobiotic stimulus; GO:0048729 tissue morphogenesis; GO:0009743 response to carbohydrate; GO:0000902 cell morphogenesis; GO:0062013 positive regulation of small molecule metabolic process
G3UXL2	Prps1l3	upregulated	0.038	2	171.35	Phosphoribosyl pyrophosphate synthetase 1-like 3	GO:0046390 ribose phosphate biosynthetic process
Q9R1P4	Psma1	upregulated	0.038	2	146.50	Proteasome endopeptidase complex	GO:0009410 response to xenobiotic stimulus
P54775	Psmc4	upregulated	0.038	2	174.61	26S proteasome regulatory subunit 6B	GO:0043161 proteasome-mediated ubiquitin-dependent protein catabolic process
Q9JMH6	Txnrd1	upregulated	0.038	6	859.34	Thioredoxin reductase 1, cytoplasmic	GO:0007369 gastrulation; GO:0048729 tissue morphogenesis; GO:0006739 NADP metabolic process; GO:0042744 hydrogen peroxide catabolic process
Q3U4W8	Usp5	upregulated	0.038	5	637.16	Ubiquitin carboxyl-terminal hydrolase	GO:2000060 positive regulation of ubiquitin-dependent protein catabolic process
P61982	Ywhag	upregulated	0.038	6	1289.78	14−3−3 protein gamma	GO:0009743 response to carbohydrate
P04117	Fabp4	upregulated	0.038	9	1175.56	Fatty acid-binding protein, adipocyte	GO:0006006 glucose metabolic process; GO:0009410 response to xenobiotic stimulus; GO:0010035 response to inorganic substance; GO:0040007 growth
Q9DBJ1	Pgam1	upregulated	0.039	3	1626.50	Phosphoglycerate mutase 1	GO:0006006 glucose metabolic process
Q9R1P1	Psmb3	upregulated	0.039	2	138.99	Proteasome subunit beta type-3	GO:0043161 proteasome-mediated ubiquitin-dependent protein catabolic process
P17751	Tpi1	upregulated	0.039	64	8158.99	Triosephosphate isomerase	GO:0006006 glucose metabolic process; GO:1901615 organic hydroxy compound metabolic process
Q6GT24	Prdx6	upregulated	0.042	6	977.71	Peroxiredoxin-6	GO:0042744 hydrogen peroxide catabolic process
P21550	Eno3	upregulated	0.042	97	24490.12	Beta-enolase	GO:0006006 glucose metabolic process
P28271	Aco1	upregulated	0.044	5	439.82	Cytoplasmic aconitate hydratase	GO:0048729 tissue morphogenesis; GO:0010035 response to inorganic substance
Q8R146	Ah	upregulated	0.044	4	300.59	Acylamino-acid-releasing enzyme (Fragment)	GO:0009410 response to xenobiotic stimulus; GO:0048729 tissue morphogenesis; GO:0000902 cell morphogenesis; GO:0040007 growth; GO:0051052 regulation of DNA metabolic process
Q921G7	Etfdh	upregulated	0.044	17	2077.99	Electron transfer flavoprotein-ubiquinone oxidoreductase, mitochondrial	GO:0006006 glucose metabolic process
Q64521	Gpd2	upregulated	0.045	24	2626.05	Glycerol-3-phosphate dehydrogenase, mitochondrial	GO:0006006 glucose metabolic process; GO:0040007 growth; GO:0006739 NADP metabolic process
P35700	Prdx1	upregulated	0.046	11	1514.14	Peroxiredoxin-1	GO:0048729 tissue morphogenesis; GO:0010035 response to inorganic substance; GO:0050900 leukocyte migration; GO:0042744 hydrogen peroxide catabolic process
P02088	Hbb-b1	upregulated	0.047	11	5054.03	Hemoglobin subunit beta-1	GO:0048729 tissue morphogenesis; GO:0042744 hydrogen peroxide catabolic process
O08677	Kng1	upregulated	0.048	6	650.50	Kininogen-1	GO:0009410 response to xenobiotic stimulus; GO:0000902 cell morphogenesis
Q9QXS1	Plec	upregulated	0.048	3	1367.54	Plectin	GO:0009410 response to xenobiotic stimulus; GO:0000902 cell morphogenesis; GO:0010035 response to inorganic substance; GO:0050900 leukocyte migration; GO:0040007 growth
Q62159	Rhoa	upregulated	0.048	3	252.95	Transforming protein RhoA (Fragment)	GO:0009410 response to xenobiotic stimulus; GO:0048729 tissue morphogenesis; GO:0009743 response to carbohydrate; GO:0007264 small GTPase mediated signal transduction; GO:0050900 leukocyte migration
P52480	Pkm	upregulated	0.048	125	18102.54	Pyruvate kinase PKM	GO:0006006 glucose metabolic process; GO:0009743 response to carbohydrate; GO:0006089 lactate metabolic process; GO:0040007 growth

https://doi.org/10.1021/acs.jproteome.4c00143
J. Proteome Res. 2024, 23, 2452−2473

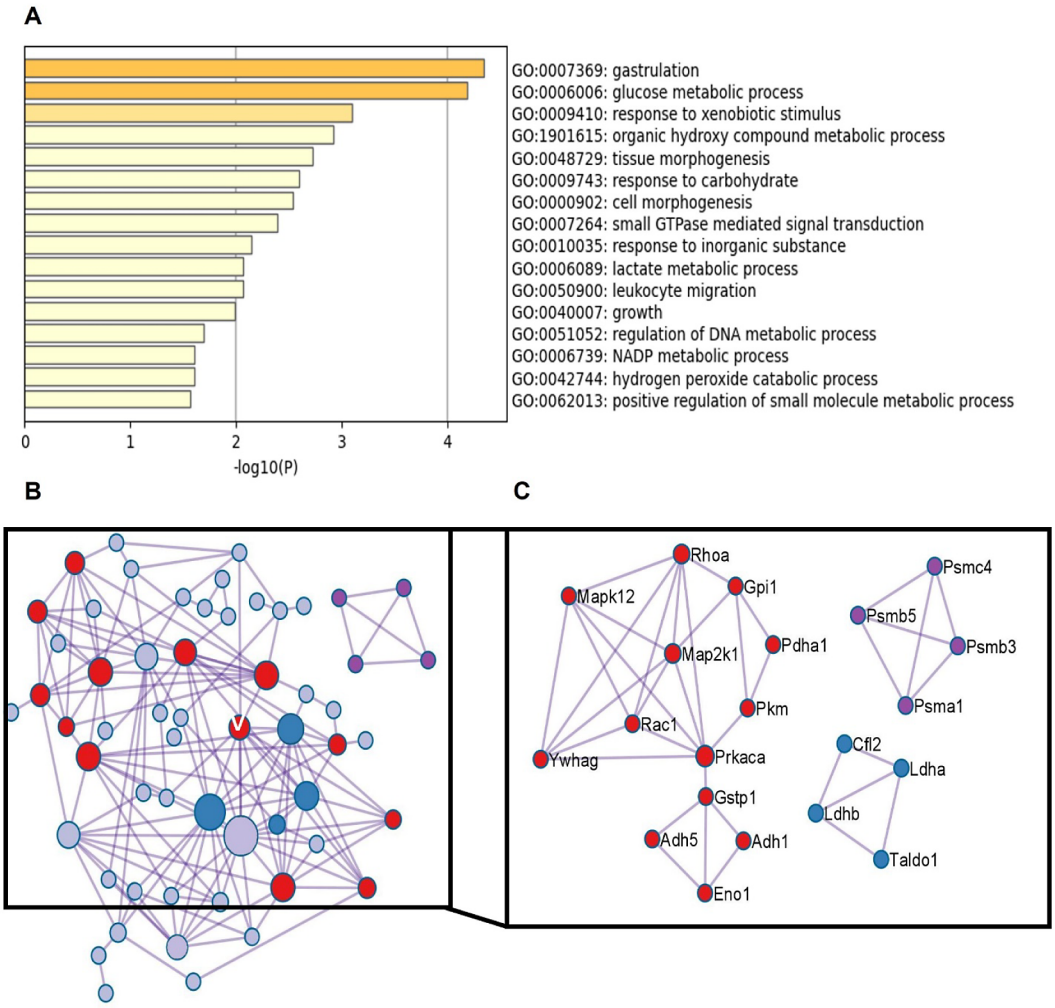

Figure 6. Proteome changes in the gastrocnemius of mice with cachexia and/or antibiotic treatment. (A) Biological processes upregulated between the C26 and C26-ATB groups. Protein−protein interactions between C26 and C26-ATB groups within the positively differentially expressed proteins (B) with a focus on three protein clusters (C). Red nodes correspond to proteins involved in protein serine threonine kinase activity, blue nodes correspond to proteins involved in pyrimidine nucleotide metabolic processes, and purple nodes to proteins involved in ubiquitin dependent protein catabolic process. C26: C26-implanted mice (n = 8), C26-ATB: C26-implanted mice treated with antibiotics (n = 7).

in our experiment. There was a strong effect of antibiotics on the muscle gastrocnemius proteome through the differential expression of growth processes—via IGF and insulin receptor pathways—and intracellular protein transport. This is coupled with a shift in the expression of proteins responsible for mitochondrial ATP synthesis, skeletal muscle contraction, and cytoskeleton organization. These alterations of the muscle proteome of mice treated with a broad spectrum of antibiotics for 2 weeks are similar to the adaptative processes put into place during aging.[26,27,65,66] HSPs, proteins involved in growth, mitochondrial energy metabolism, and sarcomere proteins such as LIM domain proteins identified here would be interesting prospects for biomarker research in the gut-muscle axis outside of cancer. Lastly, antibiotics have been widely used to replace germ-free mice in gut microbiota depletion studies. However, a study comparing antibiotic treatment (by ampicillin, neomycin, vancomycin, and metronidazole) in conventional mice and germ-free mice found that only 1/3 gene expressions were similar in the gut of the mice.[67] Treating germ-free mice and conventional mice with antibiotics led to gut gene expression changes directly caused by the drugs and not by the microbial disturbances that they generated. Thus, future results must separate the effects of the antibiotic drugs used from gut microbiota disruptions.

Effect of Microbial Dysbiosis Induced by Antibiotic Treatment on Gastrocnemius Muscle Proteomics for Mice with Cachexia

There were 80 differentially expressed proteins between C26 and C26-ATB groups, with only 4 negatively expressed and 76 positively expressed proteins (Table 5), which is less than the 143 differentially accumulated proteins obtained when microbial dysbiosis was compared in mice without cachexia. Among these proteins, only 19 common proteins were differentially accumulated in both the CT versus CT-ATB and the C26 versus C26-ATB analyses (Table S2). This first result suggests a blunted response of the muscle proteome to microbial dysbiosis induced by antibiotic treatment when cachexia is present and adaptative processes without unnecessary overlapping.

Impact on Glucose Metabolism and Oxidative Stress. Overall, among the 4 negatively, differentially expressed proteins identified in C26-ATB mice, 3 were involved with mitochondrial electron transport: ATP synthase subunits ATP5C1, ATP5PF; and COX5B (Cytochrome c oxidase subunit 5B, mitochondrial). Although the HSPs were of particular interest in the CT

https://doi.org/10.1021/acs.jproteome.4c00143
J. Proteome Res. 2024, 23, 2452−2473

groups, modification of expression of HSPs was not found in the muscles of our C26-implanted groups.

The most overrepresented GO_BP terms for the differentially accumulated proteins (Figure 6A) were responsible for muscle development ("gastrulation"; "tissue morphogenesis"; "cell morphogenesis"), and metabolic pathways, which were glucose metabolism ("glucose metabolic process"; "response to carbohydrate") and oxidative stress response (lactate metabolic process"; "NADP metabolic process"; "hydrogen peroxide catabolic process"; "organic hydroxy compound metabolic process").

This is the first study of muscle proteomics in mice with both antibiotic treatment and C26-implantation. Other proteome analyses in C26 mice without antibiotic treatment have also shown differential expression of proteins involved in glucose metabolism and oxidative stress response, mainly in mice with a more severe weight and muscle mass loss,[13,14,16] Metabolomic analyses[68] in C26 mice without antibiotic treatment have also found that the muscle of cachectic mice have increased oxidative stress, in particular nitrogen stress, and an increase in glycolysis.[69−71] In the tibialis anterior of germ-free mice, the expression of genes involved in glycolysis such as pyruvate kinase and pyruvate dehydrogenase is decreased, and this is reversed by reseeding.[43] Altogether, the pathways of oxidative stress and glucose metabolism seem to be the most promising to further explore the link between microbiota and muscle in cachexia at a moderate cachexia stage (Figure S4).

Protein−protein interaction analyses of upregulated proteins (Figures 6B,C) revealed a major cluster linked to a "cellular response to hormone stimulus". The proteins involved in the cellular response to hormone stimulus are of mainly three types. The first are Mitogen-activated protein kinases (MAP2K1, MAPK12), which are part of a pathway already modified in a proteomics study of moderate cachexia.[13]

In colon cancer MAPK12, also known as p38γ, is of particular interest, because its knockout in a mouse model of colon cancer induced by colitis lessens the tumor volume.[72] Targeting MAPK12 *in vitro* using pirfenidone, an antifibrotic drug, leads to a decrease in colon cancer cell proliferation due to proteolysis of K-RAS (V-K_i-ras2 Kirstenrat sarcoma viral oncogene homologue), one of the main oncogenes responsible for colon cancer.[73] A transcriptomic study in mice with pancreatic cancer has also found MAPK12 mediates anaerobic glycolysis induced by KRAS.[74] Since diabetic mice treated with pirfenidone (a MAPK12 blocker) display gut microbiota resembling that of control mice rather than that of their diabetic, untreated counterparts;[75] and muscle biopsies of patients with diabetes display lower gene expression of *mapk12,* this suggests a link between microbiota and muscle through glycolysis via the KRAS/p38 MAPK pathway[76] (Figure S5).

Other enzymes involved in glutathione metabolism (alcohol dehydrogenases ADH1 and ADH5; GSTP1, glutathione S-transferase P11), glycolysis, and the TCA cycle (GPI1, glucose-6-phosphate isomerase; PKM, pyruvate kinase; PDHA1, pyruvate dehydrogenase E1 component subunit alpha; ENO1, alpha-enolase). This reinforces the idea that glucose metabolism and oxidative stress are important pathways in the context of cachexia and microbial dysbiosis.

Impact on Catabolic Process. The protein−protein interaction analysis also revealed a cluster implicated in the "ubiquitin-dependent protein catabolic process" (Figure 6B,C). The proteins involved in this catabolic process are members of the proteasome complex[77] (Figure 7): PSMC4 (26S proteasome regulatory subunit 6B), PSMA1 (20S proteasome subunits alpha), PSMB3 and PSMB5 (20S proteasome subunits). Proteasome inhibition by Velcade, an antineoplasic drug approved for myeloma, can rescue the dystrophic phenotype and decrease intramuscular inflammation in mice.[78] Among the proteins identified here, *psma1* gene expression is upregulated in the immobilized hindlimbs of mice knocked out for ZEB1, a protein involved in tumor suppression, which present steeper muscle weight loss and lower muscle fiber area.[79] PSMC4 muscle-specific knocked out mice exhibit muscle atrophy,[77] with higher SERCA, MURF1, and MAFBX1 protein expressions and ultimately higher ubiquitinylated proteins in the muscle of adult mice. Altered proteolysis thus seems to be of particular interest in the double context of cancer and microbiota disruption.

Altered proteolysis thus seems of particular interest in the double context of cancer and microbiota disruption. Proteasome inhibition of PSMB5 by bortezomib, an antineoplasic drug approved for myeloma, can rescue the dystrophic phenotype and decrease intramuscular inflammation in mice.[78] This is also the case in mice treated with cisplatin, where bortezomib rescues the decrease in muscle mass and myofiber diameter. Interestingly, gut microbiota participates in bortezomib drug resistance in myeloma,[80] as humans and mice with higher *Citrobacter freundii* levels, a nitrogen recycling bacteria, display larger tumors after bortezomib treatment. Moreover, after this treatment, mice undergoing fecal microbiota transplantation of humans with relapsing myeloma presented larger tumors than mice transplanted with patients with an initial diagnosis of myeloma. Finally, administering a probiotic containing *Citrobacter butyricum* reduces *C. freundii* abundance in mice, and they have smaller tumors following bortezomib treatment than mice without probiotic gavage. Thus, in the future, modulating gut microbiota may be able to reverse bortezomib resistance and, as a result, muscle alterations.

Overall, a different response of the muscle proteome to microbiota disruption when cachexia is present was observed, suggesting that the adaptation of skeletal muscle to this catabolic condition is impaired. Only 24% proteins were commonly identified regardless of the C26 implantation status. This suggests that the muscle proteome is modified differently in control animals versus cachectic in the context of antibiotics treatment, with adaptative processes that do not completely overlap. For C26 mice with moderate cachexia submitted to antibiotic treatment, the main altered processes are glucose metabolism, oxidative stress, and proteolysis.

CONCLUSION

In this study, C26 mice presented a moderate cachexia characterized by a lowered muscle protein synthesis and an increase in the mRNA expressions of *murf1*, *mafbx*, and *klf15* together with microbial dysbiosis with an increase in *Enterobacteriaceae*. Drastically impacting microbiota with broad-spectrum antibiotics treatment did not induce additional muscle protein synthesis decline in cachectic mice. However, antibiotic treatment under cancer conditions induced a greater total weight loss compared to antibiotic-treated control mice and untreated cachectic mice, with the activation of gene expressions involved in muscle atrophy such as *mafbx*. Muscle proteomic analyses revealed a strong effect of microbial disturbances secondary to antibiotics on the muscle gastrocnemius proteome outside of cancer, with adaptative processes observed here like the ones in the context of aging. Differentially accumulated proteins were involved in BP processes, such as protein folding,

https://doi.org/10.1021/acs.jproteome.4c00143
J. Proteome Res. 2024, 23, 2452−2473

growth, and intracellular protein transport, especially HSPs. Negatively, differentially expressed proteins were involved in BP processes, such as mitochondrial ATP synthesis and electron transport, muscle contraction, and cytoskeleton organization, especially proteins with LIM domains. The adaptation of the muscle proteome secondary to microbial dysbiosis was impaired for cachectic mice compared with the control mice, with few shared proteins shifting aside from muscle metabolism. Differentially accumulated proteins were mostly involved with BP terms such as glucose and oxidative stress metabolism, muscle development, and response to xenobiotic stimulus, and clusters linked to the cellular response to hormone stimulus involving MAPK proteins, or ubiquitin-dependent protein catabolic processes. These data reveal a major effect of antibiotic treatment-induced microbial disturbances on skeletal muscle proteins regulation.

Our study is the first to explore the skeletal muscle proteome profile changes induced by antibiotic-induced microbial disturbances in the C26 mouse model and outside of cachexia. It enables the identification of potential biomarkers of an alteration of muscle−microbiota interactions at an early stage of cachexia. We find that antibiotic-mediated microbiota modulation might reduce the muscle's adaptative capacity to respond to cachexia. While we have studied the effects of antibiotics immediately after their administration, we do not know how the muscle proteome reacts in the long-term after the antibiotic treatment, and future research should explore this as well as validate our results in other models of cancer cachexia. Future nutritional strategies should consider targeting microbiota with prebiotics to minimize muscle loss both during and after cachexia.

■ ASSOCIATED CONTENT

Supporting Information

The Supporting Information is available free of charge at https://pubs.acs.org/doi/10.1021/acs.jproteome.4c00143.

Supporting Information 1. Sequencing procedures, bioinformatics, and biostatistics analyses methodology for 16S rRNA gene sequencing of fecal microbiota (PDF)
Supporting Information 2. Water intake and food intake over time across groups. Mean tibialis weight and fiber area on necropsy day across groups. Effect of antibiotic treatment on mice with or without cachexia in terms of alpha diversity and 16S rRNA gene sequencing results. Schematic of main pathways presenting proteome changes between C26 and C26-ATB mice (PDF)
Supporting Information 3. Table of modified taxa between CT and C26 mice; table comparing differentially accumulated proteins after proteomic analyses between CT and CT-ATB groups and C26 and C26-ATB groups; proteomics raw data have also been made available on the Proteome Exchange[81] platform with the following account details: Username: reviewer_pxd043918@ebi.a-c.uk Password: CYG3Khxt (PDF)

■ AUTHOR INFORMATION

Corresponding Author

Christelle Guillet − *Université Clermont Auvergne, INRAE, UNH, Unité de Nutrition Humaine, CRNH Auvergne, Université Clermont Auvergne, Clermont-Ferrand 63001, France;* orcid.org/0000-0003-3308-723X; Email: christelle.guillet@uca.fr

Authors

Mathilde Simonson − *Université Clermont Auvergne, INRAE, UNH, Unité de Nutrition Humaine, CRNH Auvergne, Université Clermont Auvergne, Clermont-Ferrand 63001, France;* Present Address: Université de la Réunion, CHU La Réunion, service de diabétologie-endocrinologie, Saint Pierre, France. Address: Service de diabétologie-endocrinologie, CHU Sud Réunion, Avenue François Mitterrand BP 350, 97448 Saint-Pierre Cedex

Gwendal Cueff − *Université Clermont Auvergne, INRAE, UNH, Unité de Nutrition Humaine, CRNH Auvergne, Université Clermont Auvergne, Clermont-Ferrand 63001, France*

Morgane M. Thibaut − *MNUT Research group, Louvain Drug Research Institute, Université catholique de Louvain, Brussels 1200, Belgium*

Christophe Giraudet − *Université Clermont Auvergne, INRAE, UNH, Unité de Nutrition Humaine, CRNH Auvergne, Université Clermont Auvergne, Clermont-Ferrand 63001, France*

Jérôme Salles − *Université Clermont Auvergne, INRAE, UNH, Unité de Nutrition Humaine, CRNH Auvergne, Université Clermont Auvergne, Clermont-Ferrand 63001, France*

Christophe Chambon − *Animal Products Quality Unit (QuaPA), INRAE, Clermont-Ferrand 63122, France; Metabolomic and Proteomic Exploration Facility, Clermont Auvergne University, INRAE, Clermont-Ferrand 63122, France*

Yves Boirie − *Université Clermont Auvergne, INRAE, UNH, Unité de Nutrition Humaine, CRNH Auvergne, Université Clermont Auvergne, Clermont-Ferrand 63001, France; CHU Clermont-Ferrandservice de Nutrition clinique, Université Clermont Auvergne, Clermont-Ferrand 63003, France*

Laure B. Bindels − *MNUT Research group, Louvain Drug Research Institute, Université catholique de Louvain, Brussels 1200, Belgium; Welbio Department, WEL Research Institute, Wavre 1300, Belgium*

Marine Gueugneau − *Université Clermont Auvergne, INRAE, UNH, Unité de Nutrition Humaine, CRNH Auvergne, Université Clermont Auvergne, Clermont-Ferrand 63001, France*

Complete contact information is available at: https://pubs.acs.org/10.1021/acs.jproteome.4c00143

Author Contributions

The manuscript was written through contributions of all authors. All authors have given approval to the final version of the manuscript.

Funding

This research was brought forth thanks to funding from the European Society for Clinical Nutrition and Metabolism (ESPEN), the Agence Régionale de Santé Auvergne Rhône Alpes, and the Wide-Open World Cap 20−25 grant system of Clermont Auvergne University.

Notes

The authors declare no competing financial interest.

■ ACKNOWLEDGMENTS

We would like to thank Martin Nicolas for his help regarding muscle qPCR experiments, and Bouazza Es Saadi for his help during the reverse transcription and qPCR experiments as well

as fecal DNA extraction and sample preparation for sequencing. We would like to thank Caroline Barbé for her help in the protein extraction from gastrocnemius muscles. We would like also to thank the whole of Pr Bindels' team for their help during the mouse necropsy.

■ ABBREVIATIONS

APC: Adenomatous Polyposis Coli; ATB: Antibiotic; cDNA: Copy Deoxyribonucleic Acid; C26: Colon Carcinoma 26; CT: Control; FSR: Fractional Synthesis Rate; IGFBP5: Insulin Growth Factor Binding Protein 5; IRS1: Insulin Receptor Substrate 1; KLF15: Krüppel-like Factor 15; MAFbx: Muscle Atrophy F-box; MuRF-1: Muscle-specific Ring Finger; PCA: Principal Component Analysis; PERMANOVA: PERMutational ANalysis of Variance; REDD1: Regulated in Development and DNA Damage 1; R-Co-A: R-Coenzyme A; Rpl6: Ribosomal Protein l6

■ REFERENCES

(1) Fearon, K.; Strasser, F.; Anker, S. D.; Bosaeus, I.; Bruera, E.; Fainsinger, R. L.; Jatoi, A.; Loprinzi, C.; MacDonald, N.; Mantovani, G.; Davis, M.; Muscaritoli, M.; Ottery, F.; Radbruch, L.; Ravasco, P.; Walsh, D.; Wilcock, A.; Kaasa, S.; Baracos, V. E. Definition and Classification of Cancer Cachexia: An International Consensus. *Lancet Oncol.* **2011**, *12* (5), 489−495.

(2) Wallengren, O.; Lundholm, K.; Bosaeus, I. Diagnostic Criteria of Cancer Cachexia: Relation to Quality of Life, Exercise Capacity and Survival in Unselected Palliative Care Patients. *Support Care Cancer* **2013**, *21* (6), 1569−1577.

(3) Baracos, V. E.; Martin, L.; Korc, M.; Guttridge, D. C.; Fearon, K. C. H. Cancer-Associated Cachexia. *Nat. Rev. Dis. Primers* **2018**, *4* (1), 17105.

(4) Hong, S.; Kim, K. W.; Park, H. J.; Ko, Y.; Yoo, C.; Park, S. Y.; Khang, S.; Jeong, H.; Lee, J. Impact of Baseline Muscle Mass and Myosteatosis on the Development of Early Toxicity During First-Line Chemotherapy in Patients With Initially Metastatic Pancreatic Cancer. *Front. Oncol.* **2022**, *12*, 878472.

(5) Okugawa, Y.; Kitajima, T.; Yamamoto, A.; Shimura, T.; Kawamura, M.; Fujiwara, T.; Mochiki, I.; Okita, Y.; Tsujiura, M.; Yokoe, T.; Ohi, M.; Toiyama, Y. Clinical Relevance of Myopenia and Myosteatosis in Colorectal Cancer. *J. Clin. Med.* **2022**, *11* (9), 2617.

(6) Acharyya, S.; Ladner, K. J.; Nelsen, L. L.; Damrauer, J.; Reiser, P. J.; Swoap, S.; Guttridge, D. C. Cancer Cachexia Is Regulated by Selective Targeting of Skeletal Muscle Gene Products. *J. Clin. Invest.* **2004**, *114* (3), 370−378.

(7) Sartori, R.; Romanello, V.; Sandri, M. Mechanisms of Muscle Atrophy and Hypertrophy: Implications in Health and Disease. *Nat. Commun.* **2021**, *12* (1), 330.

(8) Argilés, J. M.; Busquets, S.; Stemmler, B.; López-Soriano, F. J. Cancer Cachexia: Understanding the Molecular Basis. *Nat. Rev. Cancer* **2014**, *14* (11), 754−762.

(9) Dolly, A.; Dumas, J.-F.; Servais, S. Cancer Cachexia and Skeletal Muscle Atrophy in Clinical Studies: What Do We Really Know? *J. Cachexia, Sarcopenia Muscle* **2020**, *11* (6), 1413−1428.

(10) Schmidt, S. F.; Rohm, M.; Herzig, S.; Berriel Diaz, M. Cancer Cachexia: More Than Skeletal Muscle Wasting. *Trends Cancer* **2018**, *4* (12), 849−860.

(11) Ballarò, R.; Beltrà, M.; De Lucia, S.; Pin, F.; Ranjbar, K.; Hulmi, J. J.; Costelli, P.; Penna, F. Moderate Exercise in Mice Improves Cancer plus Chemotherapy-Induced Muscle Wasting and Mitochondrial Alterations. *FASEB J.* **2019**, *33* (4), 5482−5494.

(12) Samuels, S. E.; Knowles, A. L.; Tilignac, T.; Debiton, E.; Madelmont, J. C.; Attaix, D. Higher Skeletal Muscle Protein Synthesis and Lower Breakdown after Chemotherapy in Cachectic Mice. *Am. J. Physiol.* **2001**, *281* (1), R133−R139.

(13) Khamoui, A. V.; Tokmina-Roszyk, D.; Feresin, R. G.; Fields, G. B.; Visavadiya, N. P. Skeletal Muscle Proteome Expression Differentiates Severity of Cancer Cachexia in Mice and Identifies Loss of Fragile X Mental Retardation Syndrome-Related Protein 1. *Proteomics* **2022**, *22* (10), No. e2100157.

(14) Barreto, R.; Mandili, G.; Witzmann, F. A.; Novelli, F.; Zimmers, T. A.; Bonetto, A. Cancer and Chemotherapy Contribute to Muscle Loss by Activating Common Signaling Pathways. *Front. Physiol.* **2016**, *7*, 7.

(15) Bonetto, A.; Rupert, J. E.; Barreto, R.; Zimmers, T. A. The Colon-26 Carcinoma Tumor-Bearing Mouse as a Model for the Study of Cancer Cachexia. *JoVE* **2016**, *117*, 54893.

(16) Massart, I. S.; Paulissen, G.; Loumaye, A.; Lause, P.; Pötgens, S. A.; Thibaut, M. M.; Balan, E.; Deldicque, L.; Atfi, A.; Louis, E.; Gruson, D.; Bindels, L. B.; Meuwis, M.-A.; Thissen, J.-P. Marked Increased Production of Acute Phase Reactants by Skeletal Muscle during Cancer Cachexia. *Cancers* **2020**, *12* (11), 3221.

(17) Bindels, L. B.; Beck, R.; Schakman, O.; Martin, J. C.; De Backer, F.; Sohet, F. M.; Dewulf, E. M.; Pachikian, B. D.; Neyrinck, A. M.; Thissen, J.-P.; Verrax, J.; Calderon, P. B.; Pot, B.; Grangette, C.; Cani, P. D.; Scott, K. P.; Delzenne, N. M. Restoring Specific Lactobacilli Levels Decreases Inflammation and Muscle Atrophy Markers in an Acute Leukemia Mouse Model. *PLoS One* **2012**, *7* (6), No. e37971.

(18) Pötgens, S. A.; Brossel, H.; Sboarina, M.; Catry, E.; Cani, P. D.; Neyrinck, A. M.; Delzenne, N. M.; Bindels, L. B. Klebsiella Oxytoca Expands in Cancer Cachexia and Acts as a Gut Pathobiont Contributing to Intestinal Dysfunction. *Sci. Rep.* **2018**, *8* (1), 12321.

(19) Pötgens, S. A.; Thibaut, M. M.; Joudiou, N.; Sboarina, M.; Neyrinck, A. M.; Cani, P. D.; Claus, S. P.; Delzenne, N. M.; Bindels, L. B. Multi-Compartment Metabolomics and Metagenomics Reveal Major Hepatic and Intestinal Disturbances in Cancer Cachectic Mice. *J. Cachexia Sarcopenia Muscle* **2021**, *12* (2), 456−475.

(20) Costea, P. I.; Zeller, G.; Sunagawa, S.; Pelletier, E.; Alberti, A.; Levenez, F.; Tramontano, M.; Driessen, M.; Hercog, R.; Jung, F.-E.; Kultima, J. R.; Hayward, M. R.; Coelho, L. P.; Allen-Vercoe, E.; Bertrand, L.; Blaut, M.; Brown, J. R. M.; Carton, T.; Cools-Portier, S.; Daigneault, M.; Derrien, M.; Druesne, A.; de Vos, W. M.; Finlay, B. B.; Flint, H. J.; Guarner, F.; Hattori, M.; Heilig, H.; Luna, R. A.; van Hylckama Vlieg, J.; Junick, J.; Klymiuk, I.; Langella, P.; Le Chatelier, E.; Mai, V.; Manichanh, C.; Martin, J. C.; Mery, C.; Morita, H.; O'Toole, P. W.; Orvain, C.; Patil, K. R.; Penders, J.; Persson, S.; Pons, N.; Popova, M.; Salonen, A.; Saulnier, D.; Scott, K. P.; Singh, B.; Slezak, K.; Veiga, P.; Versalovic, J.; Zhao, L.; Zoetendal, E. G.; Ehrlich, S. D.; Dore, J.; Bork, P. Towards Standards for Human Fecal Sample Processing in Metagenomic Studies. *Nat. Biotechnol.* **2017**, *35* (11), 1069−1076.

(21) Ovreås, L.; Forney, L.; Daae, F. L.; Torsvik, V. Distribution of Bacterioplankton in Meromictic Lake Saelenvannet, as Determined by Denaturing Gradient Gel Electrophoresis of PCR-Amplified Gene Fragments Coding for 16S rRNA. *Appl. Environ. Microbiol.* **1997**, *63* (9), 3367−3373.

(22) Pötgens, S. A.; Lecop, S.; Havelange, V.; Li, F.; Neyrinck, A. M.; Neveux, N.; Maertens, J.; Walter, J.; Schoemans, H.; Delzenne, N. M.; Bindels, L. B. Gut Microbiota Alterations Induced by Intensive Chemotherapy in Acute Myeloid Leukaemia Patients Are Associated with Gut Barrier Dysfunction and Body Weight Loss. *Clin. Nutr.* **2023**, *42* (11), 2214−2228.

(23) Breton, J.; Tirelle, P.; Hasanat, S.; Pernot, A.; L'Huillier, C.; do Rego, J.-C.; Déchelotte, P.; Coëffier, M.; Bindels, L. B.; Ribet, D. Gut Microbiota Alteration in a Mouse Model of Anorexia Nervosa. *Clin. Nutr.* **2021**, *40* (1), 181−189.

(24) Gueugneau, M.; d'Hose, D.; Barbé, C.; de Barsy, M.; Lause, P.; Maiter, D.; Bindels, L. B.; Delzenne, N. M.; Schaeffer, L.; Gangloff, Y.; Chambon, C.; Coudy-Gandilhon, C.; Béchet, D.; Thissen, J. Increased Serpina3n Release into Circulation during Glucocorticoid-mediated Muscle Atrophy. *J. Cachexia Sarcopenia Muscle* **2018**, *9* (5), 929−946.

(25) Walrand, S.; Zangarelli, A.; Guillet, C.; Salles, J.; Soulier, K.; Giraudet, C.; Patrac, V.; Boirie, Y. Effect of Fast Dietary Proteins on Muscle Protein Synthesis Rate and Muscle Strength in *Ad Libitum* -Fed and Energy-Restricted Old Rats. *Br. J. Nutr.* **2011**, *106* (11), 1683−1690.

https://doi.org/10.1021/acs.jproteome.4c00143
J. Proteome Res. 2024, 23, 2452−2473

(26) Barbé, C.; Salles, J.; Chambon, C.; Giraudet, C.; Sanchez, P.; Patrac, V.; Denis, P.; Boirie, Y.; Walrand, S.; Gueugneau, M. Characterization of the Skeletal Muscle Proteome in Undernourished Old Rats. *Int. J. Mol. Sci.* **2022**, *23* (9), 4762.
(27) Coudy-Gandilhon, C.; Gueugneau, M.; Chambon, C.; Taillandier, D.; Combaret, L.; Polge, C.; Millet, G. Y.; Féasson, L.; Béchet, D. A Single Bout of Ultra-Endurance Exercise Reveals Early Signs of Muscle Aging in Master Athletes. *Int. J. Mol. Sci.* **2022**, *23* (7), 3713.
(28) Perez-Riverol, Y.; Csordas, A.; Bai, J.; Bernal-Llinares, M.; Hewapathirana, S.; Kundu, D. J.; Inuganti, A.; Griss, J.; Mayer, G.; Eisenacher, M.; Pérez, E.; Uszkoreit, J.; Pfeuffer, J.; Sachsenberg, T.; Yilmaz, S.; Tiwary, S.; Cox, J.; Audain, E.; Walzer, M.; Jarnuczak, A. F.; Ternent, T.; Brazma, A.; Vizcaíno, J. A. The PRIDE Database and Related Tools and Resources in 2019: Improving Support for Quantification Data. *Nucleic Acids Res.* **2019**, *47* (D1), D442−D450.
(29) Zhou, Y.; Zhou, B.; Pache, L.; Chang, M.; Khodabakhshi, A. H.; Tanaseichuk, O.; Benner, C.; Chanda, S. K. Metascape Provides a Biologist-Oriented Resource for the Analysis of Systems-Level Datasets. *Nat. Commun.* **2019**, *10* (1), 1523.
(30) Ashburner, M.; Ball, C. A.; Blake, J. A.; Botstein, D.; Butler, H.; Cherry, J. M.; Davis, A. P.; Dolinski, K.; Dwight, S. S.; Eppig, J. T.; Harris, M. A.; Hill, D. P.; Issel-Tarver, L.; Kasarskis, A.; Lewis, S.; Matese, J. C.; Richardson, J. E.; Ringwald, M.; Rubin, G. M.; Sherlock, G. Gene Ontology: Tool for the Unification of Biology The Gene Ontology Consortium. *Nat. Genet.* **2000**, *25* (1), 25−29.
(31) Bader, G. D.; Hogue, C. W. An Automated Method for Finding Molecular Complexes in Large Protein Interaction Networks. *BMC Bioinf.* **2003**, *4*, 2.
(32) Reikvam, D. H.; Erofeev, A.; Sandvik, A.; Grcic, V.; Jahnsen, F. L.; Gaustad, P.; McCoy, K. D.; Macpherson, A. J.; Meza-Zepeda, L. A.; Johansen, F.-E. Depletion of Murine Intestinal Microbiota: Effects on Gut Mucosa and Epithelial Gene Expression. *PLoS One* **2011**, *6* (3), No. e17996.
(33) Nay, K.; Jollet, M.; Goustard, B.; Baati, N.; Vernus, B.; Pontones, M.; Lefeuvre-Orfila, L.; Bendavid, C.; Rué, O.; Mariadassou, M.; Bonnieu, A.; Ollendorff, V.; Lepage, P.; Derbré, F.; Koechlin-Ramonatxo, C. Gut Bacteria Are Critical for Optimal Muscle Function: A Potential Link with Glucose Homeostasis. *Am. J. Physiol. Endocrinol. Metab.* **2019**, *317* (1), No. E158−E171.
(34) Bindels, L. B.; Neyrinck, A. M.; Loumaye, A.; Catry, E.; Walgrave, H.; Cherbuy, C.; Leclercq, S.; Van Hul, M.; Plovier, H.; Pachikian, B.; Bermúdez-Humarán, L. G.; Langella, P.; Cani, P. D.; Thissen, J.-P.; Delzenne, N. M. Increased Gut Permeability in Cancer Cachexia: Mechanisms and Clinical Relevance. *Oncotarget* **2018**, *9* (26), 18224−18238.
(35) Rakoff-Nahoum, S.; Paglino, J.; Eslami-Varzaneh, F.; Edberg, S.; Medzhitov, R. Recognition of Commensal Microflora by Toll-Like Receptors Is Required for Intestinal Homeostasis. *Cell* **2004**, *118* (2), 229−241.
(36) Tirelle, P.; Breton, J.; Riou, G.; Déchelotte, P.; Coëffier, M.; Ribet, D. Comparison of Different Modes of Antibiotic Delivery on Gut Microbiota Depletion Efficiency and Body Composition in Mouse. *BMC Microbiol.* **2020**, *20* (1), 340.
(37) Nissinen, T. A.; Hentilä, J.; Penna, F.; Lampinen, A.; Lautaoja, J. H.; Fachada, V.; Holopainen, T.; Ritvos, O.; Kivelä, R.; Hulmi, J. J. Treating Cachexia Using Soluble ACVR2B Improves Survival, Alters mTOR Localization, and Attenuates Liver and Spleen Responses: Treating Cachexia Using Soluble ACVR2B. *J. Cachexia, Sarcopenia Muscle* **2018**, *9* (3), 514−529.
(38) White, J. P.; Baynes, J. W.; Welle, S. L.; Kostek, M. C.; Matesic, L. E.; Sato, S.; Carson, J. A. The Regulation of Skeletal Muscle Protein Turnover during the Progression of Cancer Cachexia in the ApcMin/+ Mouse. *PLoS One* **2011**, *6* (9), No. e24650.
(39) Smith, K.; Tisdale, M. Increased Protein Degradation and Decreased Protein Synthesis in Skeletal Muscle during Cancer Cachexia. *Br. J. Cancer* **1993**, *67* (4), 680−685.
(40) Dworzak, F.; Ferrari, P.; Gavazzi, C.; Maiorana, C.; Bozzetti, F. Effects of Cachexia Due to Cancer on Whole Body and Skeletal Muscle Protein Turnover. *Cancer* **1998**, *82* (1), 42−48.
(41) Emery, P. W.; Edwards, R. H.; Rennie, M. J.; Souhami, R. L.; Halliday, D. Protein Synthesis in Muscle Measured in Vivo in Cachectic Patients with Cancer. *Br Med. J.* **1984**, *289* (6445), 584−586.
(42) Martin, A.; Gallot, Y. S.; Freyssenet, D. Molecular Mechanisms of Cancer Cachexia-Related Loss of Skeletal Muscle Mass: Data Analysis from Preclinical and Clinical Studies. *J. Cachexia Sarcopenia Muscle* **2023**, *14* (3), 1150−1167.
(43) Lahiri, S.; Kim, H.; Garcia-Perez, I.; Reza, M. M.; Martin, K. A.; Kundu, P.; Cox, L. M.; Selkrig, J.; Posma, J. M.; Zhang, H.; Padmanabhan, P.; Moret, C.; Gulyás, B.; Blaser, M. J.; Auwerx, J.; Holmes, E.; Nicholson, J.; Wahli, W.; Pettersson, S. The Gut Microbiota Influences Skeletal Muscle Mass and Function in Mice. *Sci. Transl. Med.* **2019**, *11* (502), No. eaan5662.
(44) Fan, L.; Hsieh, P. N.; Sweet, D. R.; Jain, M. K. Krüppel-like Factor 15: Regulator of BCAA Metabolism and Circadian Protein Rhythmicity. *Pharmacol. Res.* **2018**, *130*, 123−126.
(45) Shimizu, N.; Yoshikawa, N.; Ito, N.; Maruyama, T.; Suzuki, Y.; Takeda, S.; Nakae, J.; Tagata, Y.; Nishitani, S.; Takehana, K.; Sano, M.; Fukuda, K.; Suematsu, M.; Morimoto, C.; Tanaka, H. Crosstalk between Glucocorticoid Receptor and Nutritional Sensor mTOR in Skeletal Muscle. *Cell Metab.* **2011**, *13* (2), 170−182.
(46) Yoshida, T.; Delafontaine, P. Mechanisms of IGF-1-Mediated Regulation of Skeletal Muscle Hypertrophy and Atrophy. *Cells* **2020**, *9* (9), 1970.
(47) Sethi, V.; Kurtom, S.; Tarique, M.; Lavania, S.; Malchiodi, Z.; Hellmund, L.; Zhang, L.; Sharma, U.; Giri, B.; Garg, B.; Ferrantella, A.; Vickers, S. M.; Banerjee, S.; Dawra, R.; Roy, S.; Ramakrishnan, S.; Saluja, A.; Dudeja, V. Gut Microbiota Promotes Tumor Growth in Mice by Modulating Immune Response. *Gastroenterology* **2018**, *155* (1), 33−37.e6.
(48) Manickam, R.; Oh, H.; Tan, C.; Paramalingam, E.; Wahli, W. Metronidazole Causes Skeletal Muscle Atrophy and Modulates Muscle Chronometabolism. *IJMS* **2018**, *19* (8), 2418.
(49) Thibaut, M. M.; Sboarina, M.; Roumain, M.; Pötgens, S. A.; Neyrinck, A. M.; Destrée, F.; Gillard, J.; Leclercq, I. A.; Dachy, G.; Demoulin, J.; Tailleux, A.; Lestavel, S.; Rastelli, M.; Everard, A.; Cani, P. D.; Porporato, P. E.; Loumaye, A.; Thissen, J.; Muccioli, G. G.; Delzenne, N. M.; Bindels, L. B. Inflammation-induced Cholestasis in Cancer Cachexia. *J. Cachexia Sarcopenia Muscle* **2021**, *12* (1), 70−90.
(50) Wu, J.; Yan, Z.; Li, Z.; Yan, C.; Lu, S.; Dong, M.; Yan, N. Structure of the Voltage-Gated Calcium Channel Cav1.1 Complex. *Science* **2015**, *350* (6267), aad2395.
(51) Choi, Y.; Kwon, Y.; Kim, D.-K.; Jeon, J.; Jang, S. C.; Wang, T.; Ban, M.; Kim, M.-H.; Jeon, S. G.; Kim, M.-S.; Choi, C. S.; Jee, Y.-K.; Gho, Y. S.; Ryu, S. H.; Kim, Y.-K. Gut Microbe-Derived Extracellular Vesicles Induce Insulin Resistance, Thereby Impairing Glucose Metabolism in Skeletal Muscle. *Sci. Rep.* **2015**, *5* (1), 15878.
(52) Bäckhed, F.; Ding, H.; Wang, T.; Hooper, L. V.; Koh, G. Y.; Nagy, A.; Semenkovich, C. F.; Gordon, J. I. The Gut Microbiota as an Environmental Factor That Regulates Fat Storage. *Proc. Natl. Acad. Sci. U. S. A.* **2004**, *101* (44), 15718−15723.
(53) Bäckhed, F.; Manchester, J. K.; Semenkovich, C. F.; Gordon, J. I. Mechanisms Underlying the Resistance to Diet-Induced Obesity in Germ-Free Mice. *Proc. Natl. Acad. Sci. U. S. A.* **2007**, *104* (3), 979−984.
(54) Yan, H.; Yu, B.; Degroote, J.; Spranghers, T.; Van Noten, N.; Majdeddin, M.; Van Poucke, M.; Peelman, L.; De Vrieze, J.; Boon, N.; Gielen, I.; Smet, S. D.; Chen, D.; Michiels, J. Antibiotic Affects the Gut Microbiota Composition and Expression of Genes Related to Lipid Metabolism and Myofiber Types in Skeletal Muscle of Piglets. *BMC Vet Res.* **2020**, *16* (1), 392.
(55) Chen, Y.-M.; Wei, L.; Chiu, Y.-S.; Hsu, Y.-J.; Tsai, T.-Y.; Wang, M.-F.; Huang, C.-C. Lactobacillus Plantarum TWK10 Supplementation Improves Exercise Performance and Increases Muscle Mass in Mice. *Nutrients* **2016**, *8* (4), 205.
(56) Huang, W.-C.; Wei, C.-C.; Huang, C.-C.; Chen, W.-L.; Huang, H.-Y. The Beneficial Effects of Lactobacillus Plantarum PS128 on High-

https://doi.org/10.1021/acs.jproteome.4c00143
J. Proteome Res. 2024, 23, 2452−2473

Intensity, Exercise-Induced Oxidative Stress, Inflammation, and Performance in Triathletes. *Nutrients* **2019**, *11* (2), 353.
(57) Fisher, L. A. B.; Schöck, F. The Unexpected Versatility of ALP/Enigma Family Proteins. *Front. Cell Dev. Biol.* **2022**, *10*, 963608.
(58) Pathak, P.; Blech-Hermoni, Y.; Subedi, K.; Mpamugo, J.; Obeng-Nyarko, C.; Ohman, R.; Molloy, I.; Kates, M.; Hale, J.; Stauffer, S.; Sharan, S. K.; Mankodi, A. Myopathy Associated LDB3Mutation Causes Z-Disc Disassembly and Protein Aggregation through PKCα and TSC2-mTOR Downregulation. *Commun. Biol.* **2021**, *4* (1), 355.
(59) Zhou, Q.; Chu, P.-H.; Huang, C.; Cheng, C.-F.; Martone, M. E.; Knoll, G.; Shelton, G. D.; Evans, S.; Chen, J. Ablation of Cypher, a PDZ-LIM Domain Z-Line Protein, Causes a Severe Form of Congenital Myopathy. *J. Cell Biol.* **2001**, *155* (4), 605−612.
(60) Kampinga, H. H.; Hageman, J.; Vos, M. J.; Kubota, H.; Tanguay, R. M.; Bruford, E. A.; Cheetham, M. E.; Chen, B.; Hightower, L. E. Guidelines for the Nomenclature of the Human Heat Shock Proteins. *Cell Stress Chaperones* **2009**, *14* (1), 105−111.
(61) Elkenani, M.; Barakat, A. Z.; Held, T.; Rodrigues, D. M.; Mobarak, S.; Swarnka, S.; Adham, I. M.; Mohamed, B. A. Heat Shock Protein A4 Ablation Leads to Skeletal Muscle Myopathy Associated with Dysregulated Autophagy and Induced Apoptosis. *J. Transl. Med.* **2022**, *20* (1), 229.
(62) Sarparanta, J.; Jonson, P. H.; Kawan, S.; Udd, B. Neuromuscular Diseases Due to Chaperone Mutations: A Review and Some New Results. *Int. J. Mol. Sci.* **2020**, *21* (4), 1409.
(63) Yoshihara, T.; Naito, H.; Kakigi, R.; Ichinoseki-Sekine, N.; Ogura, Y.; Sugiura, T.; Katamoto, S. Heat Stress Activates the Akt/mTOR Signalling Pathway in Rat Skeletal Muscle. *Acta Physiol.* **2013**, *207* (2), 416−426.
(64) Senf, S. M.; Dodd, S. L.; McClung, J. M.; Judge, A. R. Hsp70 Overexpression Inhibits NF-kappaB and Foxo3a Transcriptional Activities and Prevents Skeletal Muscle Atrophy. *FASEB J.* **2008**, *22* (11), 3836−3845.
(65) Gueugneau, M.; Coudy-Gandilhon, C.; Chambon, C.; Verney, J.; Taillandier, D.; Combaret, L.; Polge, C.; Walrand, S.; Roche, F.; Barthélémy, J.-C.; Féasson, L.; Béchet, D. Muscle Proteomic and Transcriptomic Profiling of Healthy Aging and Metabolic Syndrome in Men. *Int. J. Mol. Sci.* **2021**, *22* (8), 4205.
(66) Gueugneau, M.; Coudy-Gandilhon, C.; Gourbeyre, O.; Chambon, C.; Combaret, L.; Polge, C.; Taillandier, D.; Attaix, D.; Friguet, B.; Maier, A. B.; Butler-Browne, G.; Béchet, D. Proteomics of Muscle Chronological Ageing in Post-Menopausal Women. *BMC Genomics* **2014**, *15*, 1165.
(67) Morgun, A.; Dzutsev, A.; Dong, X.; Greer, R. L.; Sexton, D. J.; Ravel, J.; Schuster, M.; Hsiao, W.; Matzinger, P.; Shulzhenko, N. Uncovering Effects of Antibiotics on the Host and Microbiota Using Transkingdom Gene Networks. *Gut* **2015**, *64* (11), 1732−1743.
(68) Cui, P.; Li, X.; Huang, C.; Li, Q.; Lin, D. Metabolomics and Its Applications in Cancer Cachexia. *Front. Mol. Biosci.* **2022**, *9*, 789889.
(69) Pin, F.; Barreto, R.; Couch, M. E.; Bonetto, A.; O'Connell, T. M. Cachexia Induced by Cancer and Chemotherapy Yield Distinct Perturbations to Energy Metabolism. *J. Cachexia Sarcopenia Muscle* **2019**, *10* (1), 140−154.
(70) Der-Torossian, H.; Wysong, A.; Shadfar, S.; Willis, M. S.; McDunn, J.; Couch, M. E. Metabolic Derangements in the Gastrocnemius and the Effect of Compound A Therapy in a Murine Model of Cancer Cachexia. *J. Cachexia Sarcopenia Muscle* **2013**, *4* (2), 145−155.
(71) QuanJun, Y.; GenJin, Y.; LiLi, W.; Yan, H.; YongLong, H.; Jin, L.; Jie, L.; JinLu, H.; Cheng, G. Integrated Analysis of Serum and Intact Muscle Metabonomics Identify Metabolic Profiles of Cancer Cachexia in a Dynamic Mouse Model. *RSC Adv.* **2015**, *5* (112), 92438−92448.
(72) Del Reino, P.; Alsina-Beauchamp, D.; Escós, A.; Cerezo-Guisado, M. I.; Risco, A.; Aparicio, N.; Zur, R.; Fernandez-Estévez, M.; Collantes, E.; Montans, J.; Cuenda, A. Pro-Oncogenic Role of Alternative P38 Mitogen-Activated Protein Kinases P38γ and P38δ, Linking Inflammation and Cancer in Colitis-Associated Colon Cancer. *Cancer Res.* **2014**, *74* (21), 6150−6160.
(73) Qi, X.; Xie, C.; Hou, S.; Li, G.; Yin, N.; Dong, L.; Lepp, A.; Chesnik, M. A.; Mirza, S. P.; Szabo, A.; Tsai, S.; Basir, Z.; Wu, S.; Chen, G. Identification of a Ternary Protein-Complex as a Therapeutic Target for K-Ras-Dependent Colon Cancer. *Oncotarget* **2014**, *5* (12), 4269−4282.
(74) Wang, F.; Qi, X.-M.; Wertz, R.; Mortensen, M.; Hagen, C.; Evans, J.; Sheinin, Y.; James, M.; Liu, P.; Tsai, S.; Thomas, J.; Mackinnon, A.; Dwinell, M.; Myers, C. R.; Bartrons Bach, R.; Fu, L.; Chen, G. P38γ MAPK Is Essential for Aerobic Glycolysis and Pancreatic Tumorigenesis. *Cancer Res.* **2020**, *80* (16), 3251−3264.
(75) Singh, H.; Miyamoto, S.; Darshi, M.; Torralba, M. G.; Kwon, K.; Sharma, K.; Pieper, R. Gut Microbial Changes in Diabetic Db/Db Mice and Recovery of Microbial Diversity upon Pirfenidone Treatment. *Microorganisms* **2020**, *8* (9), 1347.
(76) Palsgaard, J.; Brøns, C.; Friedrichsen, M.; Dominguez, H.; Jensen, M.; Storgaard, H.; Spohr, C.; Torp-Pedersen, C.; Borup, R.; De Meyts, P.; Vaag, A. Gene Expression in Skeletal Muscle Biopsies from People with Type 2 Diabetes and Relatives: Differential Regulation of Insulin Signaling Pathways. *PLoS One* **2009**, *4* (8), No. e6575.
(77) Kitajima, Y.; Tashiro, Y.; Suzuki, N.; Warita, H.; Kato, M.; Tateyama, M.; Ando, R.; Izumi, R.; Yamazaki, M.; Abe, M.; Sakimura, K.; Ito, H.; Urushitani, M.; Nagatomi, R.; Takahashi, R.; Aoki, M. Proteasome Dysfunction Induces Muscle Growth Defects and Protein Aggregation. *J. Cell Sci.* **2014**, *127* (Pt 24), 5204−5217.
(78) Gazzerro, E.; Assereto, S.; Bonetto, A.; Sotgia, F.; Scarfì, S.; Pistorio, A.; Bonuccelli, G.; Cilli, M.; Bruno, C.; Zara, F.; Lisanti, M. P.; Minetti, C. Therapeutic Potential of Proteasome Inhibition in Duchenne and Becker Muscular Dystrophies. *Am. J. Pathol.* **2010**, *176* (4), 1863−1877.
(79) Ninfali, C.; Siles, L.; Darling, D. S.; Postigo, A. Regulation of Muscle Atrophy-Related Genes by the Opposing Transcriptional Activities of ZEB1/CtBP and FOXO3. *Nucleic Acids Res.* **2018**, *46* (20), 10697−10708.
(80) Zhu, Y.; Jian, X.; Chen, S.; An, G.; Jiang, D.; Yang, Q.; Zhang, J.; Hu, J.; Qiu, Y.; Feng, X.; Guo, J.; Chen, X.; Li, Z.; Zhou, R.; Hu, C.; He, N.; Shi, F.; Huang, S.; Liu, H.; Li, X.; Xie, L.; Zhu, Y.; Zhao, L.; Jiang, Y.; Li, J.; Wang, J.; Qiu, L.; Chen, X.; Jia, W.; He, Y.; Zhou, W. Targeting Gut Microbial Nitrogen Recycling and Cellular Uptake of Ammonium to Improve Bortezomib Resistance in Multiple Myeloma. *Cell Metab.* **2024**, *36* (1), 159−175.e8.
(81) Vizcaíno, J. A.; Deutsch, E. W.; Wang, R.; Csordas, A.; Reisinger, F.; Ríos, D.; Dianes, J. A.; Sun, Z.; Farrah, T.; Bandeira, N.; Binz, P.-A.; Xenarios, I.; Eisenacher, M.; Mayer, G.; Gatto, L.; Campos, A.; Chalkley, R. J.; Kraus, H.-J.; Albar, J. P.; Martinez-Bartolomé, S.; Apweiler, R.; Omenn, G. S.; Martens, L.; Jones, A. R.; Hermjakob, H. ProteomeXchange Provides Globally Coordinated Proteomics Data Submission and Dissemination. *Nat. Biotechnol.* **2014**, *32* (3), 223−226.

https://doi.org/10.1021/acs.jproteome.4c00143
J. Proteome Res. 2024, 23, 2452−2473